

An analytical model of non-photorespiratory CO₂ release in the light and dark in leaves of C₃ species based on stoichiometric flux balance

THOMAS N. BUCKLEY^{1,2} & MARK A. ADAMS^{2,3}

¹Department of Biology, Sonoma State University, Rohnert Park, CA, USA, ²Bushfire Cooperative Research Centre, Melbourne, Victoria, Australia and ³Faculty of Agriculture, Food and Natural Resources, University of Sydney, Sydney, NSW, Australia

ABSTRACT

Leaf respiration continues in the light but at a reduced rate. This inhibition is highly variable, and the mechanisms are poorly known, partly due to the lack of a formal model that can generate testable hypotheses. We derived an analytical model for non-photorespiratory CO₂ release by solving steady-state supply/demand equations for ATP, NADH and NADPH, coupled to a widely used photosynthesis model. We used this model to evaluate causes for suppression of respiration by light. The model agrees with many observations, including highly variable suppression at saturating light, greater suppression in mature leaves, reduced assimilatory quotient (ratio of net CO₂ and O₂ exchange) concurrent with nitrate reduction and a Kok effect (discrete change in quantum yield at low light). The model predicts engagement of non-phosphorylating pathways at moderate to high light, or concurrent with processes that yield ATP and NADH, such as fatty acid or terpenoid synthesis. Suppression of respiration is governed largely by photosynthetic adenylate balance, although photorespiratory NADH may contribute at sub-saturating light. Key questions include the precise diel variation of anabolism and the ATP : 2e⁻ ratio for photophosphorylation. Our model can focus experimental research and is a step towards a fully process-based model of CO₂ exchange.

Key-words: alternative oxidase; carbon metabolism; Kok effect; photorespiration; photosynthesis; respiration.

Abbreviations: *A*, net CO₂ assimilation rate; *A_o*, net O₂ evolution rate; *AOX*, alternative oxidase; *B_n*, net anabolic NADH supply; *B_p*, net anabolic NADPH demand; *B_t*, net anabolic ATP demand; *c_i*, intercellular CO₂ partial pressure; *COX*, cytochrome oxidase; *f_m*, fraction of photorespiratory NADH that remains in mitochondria; *f_x*, fraction of excess thylakoid reducing potential dissipated as NADPH export; *G6PDH*, glucose-6-phosphate dehydrogenase; *I*, incident PPFD; *J*, potential thylakoid e⁻ transport rate; *J'*, *V_c* in RuBP-limiting conditions; *J_a*, actual thylakoid e⁻ transport

rate; *J_m*, max potential thylakoid e⁻ transport rate; *M*, maintenance ATP demand; *mETC*, mitochondrial e⁻ transport chain; *O*, ambient O₂ partial pressure; *OPPP*, oxidative pentose phosphate pathway; *p_e*, ATP : 2e⁻ ratio, ADP phosphorylated per 2 e⁻ transported to ferredoxin; *p_o*, P : O ratio, ratio of ADP phosphorylation to O₂ reduction in mitochondria; *p_{om}*, overall max P : O ratio; *p_{om,ana}*, max P : O ratio for NADH generated in anabolic C flow; *p_{om,cat}*, max P : O ratio for NADH derived from catabolic substrate oxidation; *p_{om,cyt}*, max P : O ratio for cytosol derived NADH; *p_{om,mtx}*, max P : O ratio for matrix derived NADH; *PPFD*, photosynthetic photon flux density; *QY*, quantum yield of CO₂ from incident PPFD; *R_c*, rate of non-photorespiratory CO₂ release; *R_o*, rate of O₂ reduction by mitochondria; *RuBP*, ribulose-1,5-bisphosphate; *S*, net conversion of TP to sucrose and/or starch; *t*, net ATP demand resulting from *S*; *TP*, triose phosphate; *V_{ana}*, rate of C flow into C skeletons for biosynthesis; *V_{by}*, rate of CO₂ release due to anabolic substrate oxidation; *V_c*, rate of RuBP carboxylation; *V_{cat}*, rate of CO₂ release due to catabolic substrate oxidation; *V_m*, maximum RuBP carboxylation rate; *V_o*, RuBP oxygenation rate; *V_{opp}*, CO₂ release rate from substrate oxidation via *OPPP*; *V_{px}*, photoreductant export rate; *W_c*, *V_c* in RuBP-saturated conditions; *α-KG*, alpha ketoglutarate; *φ*, ratio of *V_o*/*V_c*.

INTRODUCTION

At present, there is a clear and notable incongruity between the treatments of photosynthesis and respiration in models of plant gas exchange and growth, at all scales from the cellular to the ecosystem. Photosynthesis is usually predicted in C₃ plants by the model of Farquhar, von Caemmerer & Berry (1980) (FCB), whereas respiration is usually predicted empirically, for example, as a function of leaf nitrogen or ribulose 1·5-bisphosphate carboxylase/oxygenase (Rubisco) content (Williams *et al.* 1996; de Pury & Farquhar 1997), as a constant fraction of gross carbon gain (Waring, Landsberg & Williams 1998; DeLucia *et al.* 2007), as a function of tissue pool size (Running & Coughlan 1988) or in relation to phenological state, based on empirical partitioning of respiration into growth and maintenance terms (Thornley 1970; Amthor *et al.* 1994).

Correspondence: T. N. Buckley. Fax: +1 707 664 4046 (f); e-mail: tom_buckley@alumni.jmu.edu

This incongruity is clearly undesirable, and for many obvious reasons (Amthor 2000; Cannell & Thornley 2000). As an example, phenomenological models cannot be reliably extrapolated to future climate conditions or management scenarios. They are also very limited in their ability to stimulate research through generation of testable hypotheses, and they cannot as readily incorporate new knowledge as might a process model.

Phenomenological models for respiration are also increasingly untenable in light of the mounting evidence for significant interactions among mitochondrial and chloroplastic energy and carbon metabolism (Krömer 1995; Hoefnagel, Atkin & Wiskich 1998). For example, non-photorespiratory CO₂ efflux, R_c , continues in the light but typically at a lower rate than in the dark (Brooks & Farquhar 1985; Kirschbaum & Farquhar 1987; Bloom *et al.* 1989; Villar, Held & Merino 1995). Several explanations for reduced R_c in the light have been proposed, most of which involve photosynthesis to some degree: (1) Excess ATP or redox equivalents generated by the light reactions of photosynthesis can help satisfy cellular ATP demand, permitting a reduced rate of respiratory substrate oxidation. In full sunlight, chloroplasts may rely on the mitochondrial electron transport chain (mETC) as an electron sink to oxidize photoreductant, limiting photoinhibition (Krömer, Stitt & Heldt 1988; Krömer & Heldt, 1991a; Saradadevi & Raghavendra 1992; Hurry *et al.* 1996); (2) Biosynthesis of fatty acids, amino acids, phenolics and many other metabolites and compounds, requires NADPH, which in darkness is supplied by the chloroplastic oxidative pentose phosphate pathway (OPPP). Photosynthetically derived NADPH could satisfy these anabolic demands, permitting reduced CO₂ release in the OPPP; (3) Photorespiration drives NADH production via Gly decarboxylation in mitochondria; subsequent reduction of hydroxypyruvate in peroxisomes also requires NADH, yet mitochondria seemingly meet less than half of that demand (Krömer & Heldt 1991b). Any NADH remaining in mitochondria would supplant the NADH yield of catabolic substrate oxidation, permitting less CO₂ release; and (4) Oxidation of substrates to provide carbon skeletons for anabolic products typically generates more NADH than it consumes. This could also offset catabolic NADH production such that up-regulation of biosynthesis in the light could reduce CO₂ release.

The Kok effect – a discrete reduction in the quantum yield, typically somewhere near the light compensation point – is another phenomenon that is expressed in the combined effects of light on R_c (Kok 1948). Early experiments found no Kok effect in low oxygen, suggesting a role for photorespiration (Cornic & Jarvis 1972; Ishii & Murata 1978), but later, experiments at high CO₂ found the effect, arguing against such a role (Sharp, Matthews & Boyer 1984; Kirschbaum & Farquhar 1987). The current consensus is that the Kok effect results from a partial inhibition of R_c at very low light (Sharp *et al.* 1984; Kirschbaum & Farquhar 1987). It remains unclear why this inhibition is relieved so sharply at irradiances *c.* 10–20 $\mu\text{mol m}^{-2} \text{s}^{-1}$, given that R_c continues to decline as irradiance increases up to 200 $\mu\text{mol m}^{-2} \text{s}^{-1}$ or more (Brooks & Farquhar 1985; Atkin *et al.* 2000).

There is much to gain from a better and more integrated understanding of these phenomena. As these interactions may not dramatically affect the shape of the responses of net CO₂ assimilation rate (A) to CO₂ or light intensity, fitting biochemical models of photosynthesis to response curves may lead to incorrect inferences about photosynthetic parameters and behaviour. In addition, there are ample reasons to suggest that the factors that reduce R_c in the light may vary in strength over time and as environmental and phenological conditions change. For example, the rate of photorespiration is strongly dependent on temperature (Jordan & Ogren 1984; Brooks & Farquhar 1985), and the demand for reducing power and carbon skeletons varies strongly with growth rates, and therefore with season and phenology (e.g. Lambers, Chapin & Pons 2008).

A more integrated approach to modelling leaf carbon metabolism can be informed by elements of existing paradigms. For example, the scaling of respiration with tissue nitrogen content reflects the large respiratory costs of nitrate reduction, amino acid synthesis and protein assembly. Separation of respiration into growth and maintenance components is potentially useful because reductant and energy demands of growing and mature tissues are quite different, both qualitatively and quantitatively. This approach has been hard to implement in practice (Amthor 2000). A third approach, pioneered in a landmark study by Penning de Vries, Brunsting & Van Laar (1974), is the notion of stoichiometric flux balance. This approach recognizes that catabolic and anabolic carbon flows – and the associated CO₂ and O₂ flows – are quantitatively coupled to one another by the cycling of metabolic intermediates, including reductants and adenylates.

The flux balance approach works as follows: Net flows of carbon from carbohydrate sources into anabolic products are taken as inputs. Known stoichiometries of intervening pathways and cycles link those carbon flows to CO₂ release and O₂ consumption (for example, CO₂ is released in catabolic oxidation of substrates to generate ATP or NADPH for anabolism). By assuming that metabolic intermediates in those pathways and cycles are in a steady state – i.e. the flux into each intermediate pool is balanced by the flux out of that pool, regardless of the magnitude of these fluxes – one can infer total net fluxes of energy, CO₂ and O₂ associated with anabolic carbon flow. Penning de Vries *et al.* used this approach to evaluate the metabolic costs of plant tissue construction.

Here, we outline and test a model of non-photorespiratory CO₂ efflux that builds upon the flux balance approach of Penning de Vries *et al.* A significant difference is that we include photosynthesis and photorespiration in the spectrum of metabolic processes that influence CO₂ and O₂ fluxes. We formally derive a set of equations for steady-state reductant and adenylate supply and demand, and solve them to give a closed form (analytical) model for CO₂ release. In the next section, we briefly describe how we derived, parameterized and applied the model for this paper (details are given in an Appendix and in Supporting Information). The rest of the paper describes

a series of simulations and model experiments. The purpose of our simulations was to assess the relative importance of different factors believed to play a role in the suppression of CO₂ release by light.

THE MODEL

Overview

The model is derived by creating flux balance equations for ATP, NADH, chloroplastic NADPH and cytosolic NADPH and solving them for net non-photorespiratory CO₂ release. Each equation consists of numerous terms representing sources and sinks for ATP, NADH, etc. These terms, which are defined formally in the Appendix, are listed in Table 1, illustrated diagrammatically in Fig. 1 and summarized below.

ATP

The ATP flux balance equation includes terms for net ATP demand by biosynthetic reactions, maintenance processes, the Calvin cycle and photorespiration, and terms for ATP supply from photophosphorylation, glycolysis and the TCA cycle and oxidative phosphorylation. ATP yield from anabolic carbon flow through glycolysis and the TCA cycle is included in the biosynthetic demand term, which is thus a net value.

NADH

The equation for net NADH demand includes one consumption term (representing NADH oxidation at the

mETC) and four supply terms: glycolysis and the TCA cycle, export of excess chloroplastic NADPH to cytosolic NADH via the Mal/OAA shuttle, biosynthetic reactions (which, on balance, produce more NADH than they consume) and photorespiratory Gly decarboxylation in mitochondria. Some of the photorespiratory NADH is shuttled to peroxisomes for hydroxypyruvate reduction, while a fraction remains in mitochondria; that fraction is represented as a parameter (f_m) in the model.

Chloroplastic NADPH

The equation for chloroplastic NADPH includes demand terms for biosynthetic processes localized within chloroplasts, the Calvin cycle, export of excess photo-reductant at high light and export of reductant to supply the balance of photorespiratory hydroxypyruvate reduction demand in peroxisomes. There are two supply terms: thylakoid electron transport and the chloroplastic OPPP.

Cytosolic NADPH

The equation for cytosolic NADPH includes biosynthetic demands localized within the cytosol and supply from the cytosolic OPPP. The leaf composition data used to estimate anabolic demands for this paper do not include any anabolic products requiring cytosolic NADPH, so this equation is included only for completeness; it has no bearing on the simulations or analysis shown in this paper.

Table 1. Supply and demand terms in the flux-balance equations for ATP, NADH and NADPH

Energy carrier	Demand terms		Supply terms	
	Symbol	Description	Symbol	Description
ATP	B_t	Net biosynthetic demand ^b	$2p_oR_o$	Oxidative phosphorylation ^a
	M	maintenance ^b	V_{cat}	glycolysis and TCA cycle ^a
	$3V_c$	Calvin cycle ^c	$0.5p_oJ_a$	photophosphorylation ^d
	$3V_o$	Photorespiration ^c		
	tS	carbohydrate storage/access ^d		
NADH	$2R_o$	Mitochondrial electron transport ^a	B_n	Net biosynthetic supply ^b
			$2V_{cat}$	glycolysis & TCA cycle ^a
chloroplastic NADPH			V_{px}	chloroplast redox export ^a
	B_p	Net biosynthetic demand ^b	$0.5f_mV_o$	photorespiratory glycine decarboxylation ^c
	$2V_c$	Calvin cycle ^c		
	$2V_o$	Photorespiration ^c	$2V_{opp}$	Chloroplast oxidative pentose phosphate pathway ^a
	$0.5f_mV_o$	export for photorespiratory hydroxypyruvate reduction ^c	$0.5J_a$	thylakoid electron transport ^d
cytosolic NADPH	V_{px}	chloroplast redox export ^a		
	B_c	Net biosynthetic demand ^b	$2V_{opc}$	Cytosolic oxidative pentose phosphate pathway ^a

Symbols are defined formally in Tables 2 and 3. Flux balance equations are derived and given in the Appendix.

Superscripts indicate ^astate variables in the model; ^bvariables or parameters specified as model inputs; ^cvariables calculated from the FCB model; ^d J_a , actual thylakoid electron transport rate, and carbohydrate storage/access ATP cost, tS , are composite variables that include model inputs, model state variables and variables from the FCB model.

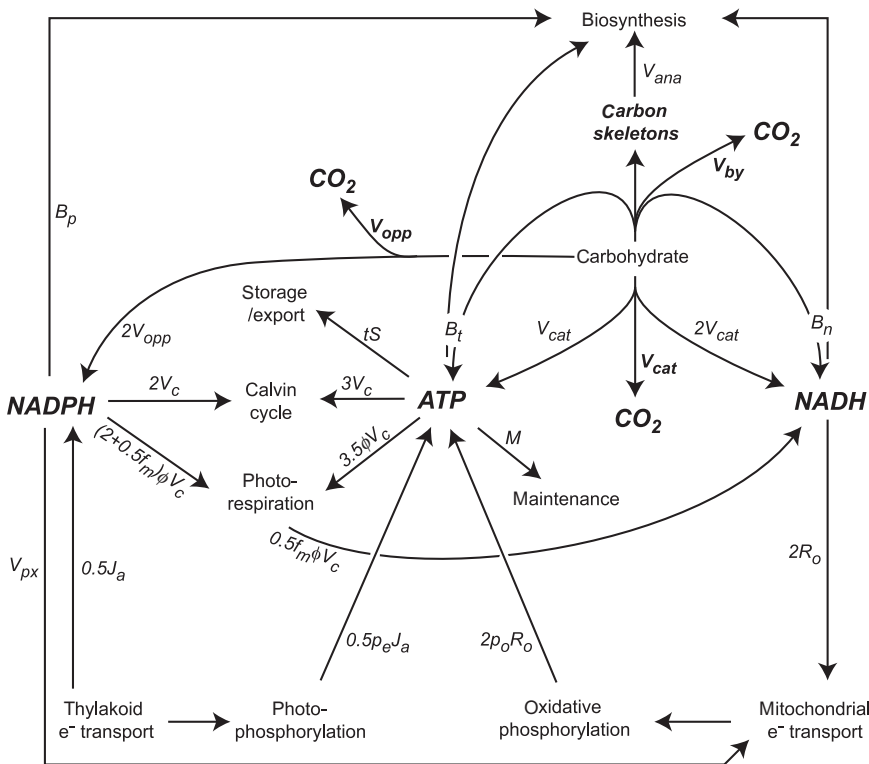


Figure 1. Diagram of the model. Heuristic diagram of the major fluxes of NADPH, ATP and NADH represented in the model, as they affect the major components of non-photorespiratory CO₂ release. Mathematical expressions for fluxes are given to assist the reader in interpreting the model derivation in the Appendix. Symbols are defined in Tables 2 and 3 and formal equations applying these quantities are developed in the Appendix and Supporting Information.

Carbon flows and CO₂ release

Several of the supply/demand terms described above are linked to CO₂ release. We capture this by expressing those terms in relation to carbon flows. These flows are ordinated in a mathematically convenient, but perhaps non-intuitive way that needs explanation. The first is the flow of carbon from a carbohydrate source (sucrose, starch or triose phosphate [TP]) into anabolic products; this is given the symbol 'V_{ana}' and is a model input, calculated from estimated anabolic demands as discussed in the Supporting Information. Although CO₂ is released as a by-product of anabolic carbon flow, the amount varies depending on the spectrum of anabolic products. Thus, we define a second carbon flow to capture this by-product CO₂ release; this is given the symbol 'V_{by}' and is also a model input estimated from anabolic demands. An important point is that some anabolic processes also consume CO₂ (e.g. generation of OAA by PEP carboxylation); these CO₂ sinks are included in V_{by}, which is thus a net value. The third carbon flow is CO₂ release from substrate oxidation in pyruvate conversion and the TCA cycle. This is given the symbol 'V_{cat}' for 'catabolic'. It includes carbon flow through these reactions *only where all of the source carbon atoms end up as CO₂*. Therefore, V_{cat} = 0 does not imply the absence of glycolysis or TCA cycle activity: carbon may continue to flow through those reactions to satisfy anabolic demands, but such carbon flow is captured in V_{ana}. The fourth flow is the net oxidation of carbohydrate to CO₂ in the chloroplastic OPPP for NADPH generation; this flow is denoted 'V_{opp}'. The fifth is oxidation of carbohydrate to CO₂ in the cytosolic OPPP, denoted 'V_{opc}'.

This separation of carbon flows into distinct streams does not represent any separation of biochemical reactions in space or time; rather, it is a convenient mathematical construction, analogous to parsing a thermodynamic change into adiabatic and isothermal steps.

Anabolic and maintenance terms

The anabolic supply/demand terms for ATP, NADH, chloroplastic and cytosolic NADPH and CO₂ (B_t, B_n, B_p, B_c and V_{by}, respectively), and the maintenance ATP demand term (M), are specified as model inputs. A brief description of how we generated these inputs follows (details are given in the Supporting Information).

First, we used published data to estimate leaf composition in terms of non-labile anabolic product contents (proteins, lignin and soluble phenolics, total carbohydrates and organic acids). Second, we converted these leaf composition data into six alternative sets of anabolic and maintenance-related demand terms by using published turnover rates for these products and estimated relative growth rates for leaves. The six sets represented two alternative scenarios for nitrogen supply to leaves (nitrate and ammonium; the former requires additional energy for assimilation), two leaf maturity levels (young and mature, represented by high and low leaf relative growth rates, respectively) and two alternatives for the 'mature' values (one of which is augmented by amino acid synthesis to represent export to other tissues). Finally, we used simplified biosynthetic stoichiometries for the biochemical components represented in these leaf composition data to estimate the net ATP, NADH, NADPH and CO₂ demands arising from anabolism to

Table 2. Anabolic and maintenance supply/demand parameters specified as inputs to the model

Parameter	Symbol	Young	Mature,exp	Mature	Dimensions
C flow into anabolic products	V_{ana}	1.8912	0.6168	0.3886	$\mu\text{mol C m}^{-2} \text{s}^{-1}$
CO ₂ release as anabolic byproduct	V_{by}	0.2012	0.0556	0.0591	$\mu\text{mol CO}_2 \text{ m}^{-2} \text{s}^{-1}$
Anabolic ATP demand	B_i	1.2742	0.3076	0.2489	$\mu\text{mol ATP m}^{-2} \text{s}^{-1}$
Maintenance ATP demand	M	1.1707	1.1707	1.1707	$\mu\text{mol ATP m}^{-2} \text{s}^{-1}$
Anabolic NADH supply (NO ₃ ⁻)	B_n	0.2695	0.1642	0.112	$\mu\text{mol NADH m}^{-2} \text{s}^{-1}$
Anabolic NADH supply (NH ₄ ⁺)		0.4539	0.2827	0.1639	$\mu\text{mol NADH m}^{-2} \text{s}^{-1}$
Anabolic NADPH demand (NO ₃ ⁻)	B_p	0.9612	0.5458	0.2798	$\mu\text{mol NADPH m}^{-2} \text{s}^{-1}$
Anabolic NADPH demand (NH ₄ ⁺)		0.4082	0.1904	0.1243	$\mu\text{mol NADPH m}^{-2} \text{s}^{-1}$

The three columns represent different phenological states (young leaves [*young*], mature leaves exporting amino acids [*mature,exp*] and mature non-exporting leaves [*mature*]). Two values are given in each case for B_n and B_p , based on nitrogen assimilation beginning from NO₃⁻ or NH₄⁺. Cytosolic NADPH demand, B_c , is not included because the leaf composition dataset used to generate these parameters did not include any products requiring cytosolic NADPH. The terms for NADH (B_n) and CO₂ (V_{by}) are given as net supply rather than net demand.

support leaf growth and maintenance (and, in the ‘exporting’ scenarios, amino acid synthesis for export). The different biosynthetic demands captured by these six alternatives lead to different relative and absolute fluxes of energy carriers, CO₂ and O₂, and these differences in turn affect the components of respiration and their quantitative interactions with photosynthesis and photorespiration. For example, fast-growing leaves have a large demand for reductant for *de novo* synthesis of amino acids and membrane phospholipids, whereas mature non-exporting leaves release CO₂ mainly through substrate oxidation to generate ATP for maintenance processes (protein reassembly and ion pumping). The demand terms are given in Table 2.

Solution of the model

The method of solving the model can be understood in two ways: parity of variables and constraints, or the steps involved in resolving these variables and constraints. Below, we briefly explain the solution from each of these viewpoints (details are given in the Appendix).

There are four explicit flux-balance equations (ATP, NADH and chloroplastic and cytosolic NADPH) and six degrees of freedom (three carbon flows – V_{opp} , V_{opc} and V_{cat} – plus O₂ reduction rate [R_o], photoreductant export rate [V_{px}] and the mitochondrial P : O ratio [p_o]; p_o is the number of ADP phosphorylated per O reduced in the mETC). All other variables are either calculated directly from the FCB model or specified as model inputs or parameters. Two additional constraints are therefore needed. We create one by applying flux balance to the relationship between chloroplastic OPPP activity and thylakoid electron transport. Specifically, since these two NADPH sources would, in the light, be linked by a futile cycle of CO₂ release and fixation, we hypothesize that carbon flow through the chloroplastic OPPP is down-regulated in proportion to increasing photoreductant supply at very low light. This constrains V_{opp} as a unique function of potential electron transport rate (J) and anabolic demand for chloroplastic NADPH (B_p). To create the sixth constraint, we hypothesize that p_o can decline below its theoretical maximum value to maintain

flux balance when NADH supply (i.e. potential mitochondrial electron transport rate) exceeds ADP supply (i.e. potential oxidative phosphorylation rate). This assumes that non-phosphorylating pathways can be variably engaged to maintain electron transport when ADP supply is limited.

The algebraic mechanics of solution involve several steps. First, we assume that cytosolic NADPH supply and demand are balanced by regulation of cytosolic OPPP activity; i.e. $V_{opc} = B_c$. Second, we constrain chloroplastic OPPP activity (V_{opp}) as discussed above, to reflect the hypothesized down-regulation of V_{opp} when photoreductant is available. This leaves one free variable in the chloroplastic NADPH flux balance equation: photoreductant export (V_{px}). The third step is therefore to solve that equation for V_{px} ; this reconciles photoreductant flux balance with the potential for NADPH supply to exceed local demand at high light. The fourth step is to apply that solution for V_{px} to the NADH equation, leaving two free variables in the NADH equation: O₂ consumption (R_o) and catabolic carbon flow (V_{cat}). The fifth step is to solve that equation for R_o as a function of V_{cat} . The sixth step is to apply the expressions for R_o and V_{px} to the ATP equation, leaving it with two variables: V_{cat} and p_o . The seventh step is to solve that equation for V_{cat} as a function of p_o . Finally, p_o is constrained by assuming it equals its theoretical maximum value unless this would require V_{cat} to be negative, in which case V_{cat} is assumed to be zero and p_o is assumed to decline as needed to satisfy the equation (i.e. to maintain flux-balance). With all free variables thus constrained, net non-photorespiratory CO₂ release (R_c) can be calculated by summing the variables linked to CO₂ release ($R_c = V_{cat} + V_{opp} + V_{opc} + V_{by}$). These steps are elaborated in the Appendix.

ANALYSIS OF THE MODEL'S PREDICTIONS REGARDING CHANGES IN R_c WITH PHOTOSYNTHETIC PHOTON FLUX DENSITY

Methods

To assess the relative contribution of different factors to the suppression of CO₂ release in the light, we performed a

series of simulations with the model. Photosynthetic photon flux density (PPFD) was the independent variable in most cases. Simulations were repeated using each of the six sets of anabolic/maintenance demand terms (B_n , B_p , B_t , V_{by} and M) described above. Additionally, we investigated the effect of possible up-regulation of anabolic demands in the light by repeating these simulations with anabolic demand terms four times greater in the light than in darkness (and with their absolute values adjusted to maintain the same diel totals, assuming a 12-hour day). Other simulations varied parameters related to photosynthesis: intercellular CO_2 partial pressure (c_i), O_2 partial pressure (O), the ATP : $2e^-$ ratio for photophosphorylation (p_e , the number of ATP generated per two electrons flowing in the linear thylakoid electron transport chain) and the fraction of photorespiratory NADH that remains in mitochondria (f_m). The results of these simulations are described below.

General behaviour of the model

Predicted values for R_c and R_o in darkness and in high light ($1000 \mu\text{mol m}^{-2} \text{s}^{-1}$), % inhibition of R_c in high light relative to darkness, net CO_2 assimilation rate (A) at high light and the ratio of net CO_2 efflux to net O_2 consumption in darkness and in high light (respiratory and assimilatory quotients, RQ and AQ, respectively) are given in Table 4 for the alternative anabolic demand scenarios outlined above. R_c varied from 0.06 to $1.11 \mu\text{mol m}^{-2} \text{s}^{-1}$ among these simulations, generally scaling with anabolic demands: for instance, R_c was greatest in the dark for young leaves supplied with nitrate, with anabolic demands equal in the light and dark. Inhibition of R_c in full light ranged from 23.9 to 81.8% for young leaves, from 64.9 to 90.0% for mature/exporting leaves and from 62.6 to 86.0% for mature/non-exporting leaves. R_c was predicted to be less inhibited by light in NH_4^+ - than in NO_3^- -fed plants, because R_c in the dark was lower in NH_4^+ . Mitochondrial O_2 reduction (R_o) was also greatest in young leaves, but in contrast to R_c , R_o was greater when NH_4^+ rather than NO_3^- was the N source. As a result, RQ and AQ were much closer to unity when leaves were supplied with NH_4^+ than when supplied with NO_3^- (e.g. 1.31 versus 1.98 for RQ in young leaves). The strongest determinant of inhibition of R_c in the light, however, was the extent to which anabolism is assumed to continue in the dark. Figure 2 shows that the proportional inhibition of R_c increases in saturating fashion with nocturnal anabolic rate (expressed as a fraction of the diurnal rate).

These point comparisons mask the dynamic response of R_c with respect to PPFD. Figure 3 shows R_c and net CO_2 assimilation rate, A , as functions of PPFD for the same permutations of conditions used to generate Table 4. In most cases, the model predicts an initial rapid decline in R_c at low light ($<20 \mu\text{mol m}^{-2} \text{s}^{-1}$), followed by a slower decline until light intensity reaches approximately $40\text{--}80 \mu\text{mol m}^{-2} \text{s}^{-1}$. The steep decline results from our model's assumption that the chloroplastic OPPP is progressively suppressed as reducing power becomes available from photosynthetic electron transport; the

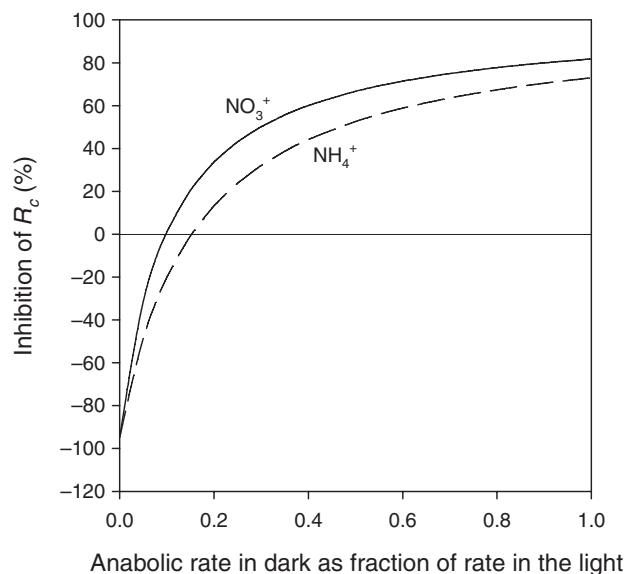


Figure 2. Effect of nocturnal anabolic rate on light suppression of respiration. Percent inhibition of non-photorespiratory CO_2 release, R_c , at saturating PPFD ($1000 \mu\text{mol m}^{-2} \text{s}^{-1}$) is shown for two scenarios: assuming nitrogen is supplied as nitrate (solid line) or ammonium (dashed line). Each line consists of a series of simulations, each of which assumed that anabolic rate in the light was a different fraction of anabolic rate in the dark (between zero and one, shown on the horizontal axis). The left end of each line represents a leaf in which anabolism occurs only in the light; the right end represents a leaf in which anabolic rates are equal in the light and dark. All other parameters are as given in Tables 2 and 3.

subsequent decline is less steep because suppression of CO_2 release in OPPP, as represented in the model, has a higher quantum yield than assimilation of CO_2 in the Calvin cycle. During the initial steep decline, R_c is greater for NO_3^- - than NH_4^+ -fed leaves because nitrate assimilation requires substrate oxidation to supply reductant. This difference quickly disappears as PPFD increases, because photosynthesis can provide the necessary reductant, and then the difference reverses because NO_3^- assimilation consumes photoreductant, leaving less excess photoreductant to suppress catabolic substrate oxidation, as required by flux-balance. However, net assimilation rates are still faster in NH_4^+ -fed leaves. In the following sections, we discuss these features as they arise in relation to different mechanisms for the suppression of R_c by light.

Role of excess photoreductant and photorespiratory NADH

We assessed the significance of two photosynthesis-related reductant flows – excess NADPH from chloroplasts, and photorespiratory NADH retained in mitochondria – in the suppression of R_c by light by comparing the relationship between R_c and PPFD under different sets of conditions chosen to modulate the rate and significance of photorespiration (Fig. 4): three values of f_m (0, 0.5 and 1), c_i (10, 25,

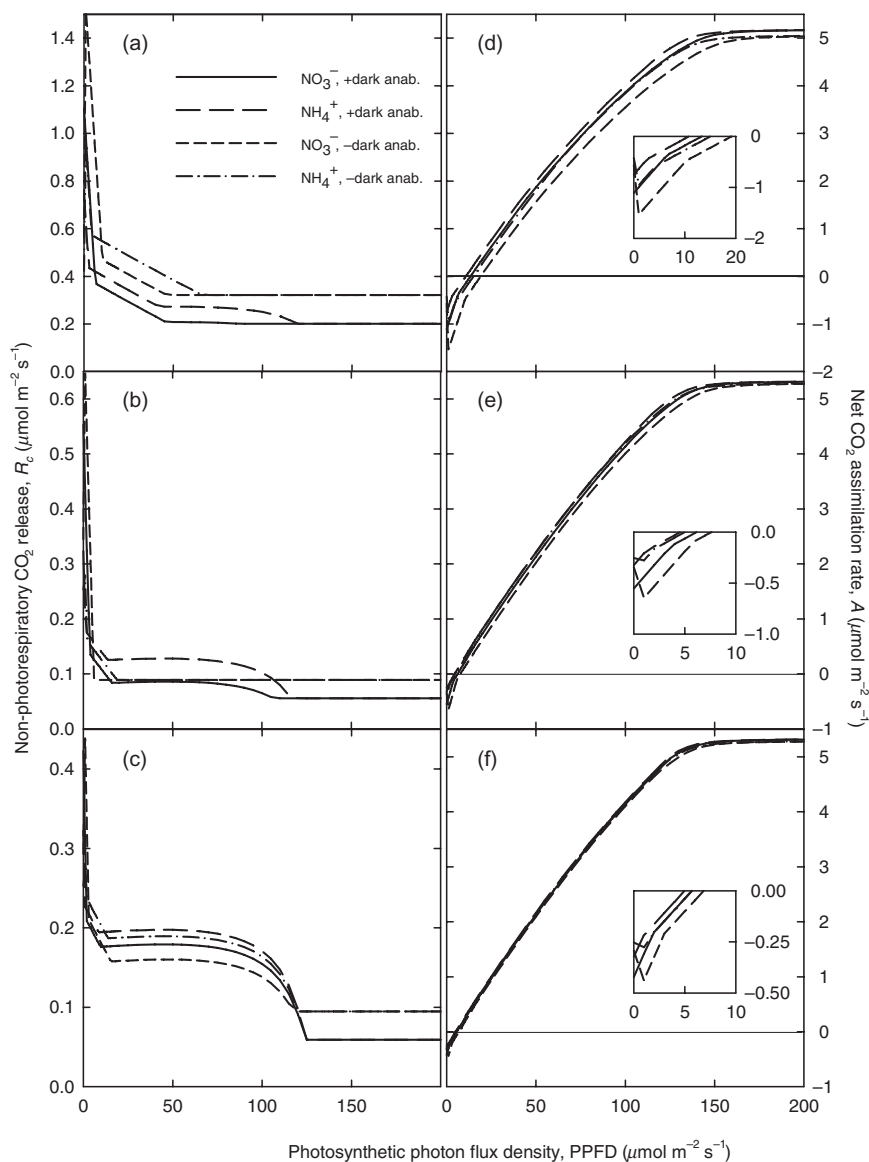


Figure 3. Effect of anabolism on response of respiration and net CO₂ assimilation to light. Non-photorespiratory CO₂ efflux, R_c (a–c) and net CO₂ assimilation rate, A (d–f) versus PPFD for different simulated regimes of anabolic demand, as affected by three factors: leaf age, enhancement of anabolism in the light and synthesis of amino acids for export. The assumptions are as follows: (a, d) young leaves, (b, e) mature exporting leaves, (c, f) mature non-exporting leaves. Solid and long-dashed lines: anabolic demands equal in light and dark; short-dashed and dash-dot lines: anabolism four times higher in the light (absolute rates adjusted to preserve diel output). Solid and short-dashed lines: N assimilation from nitrate; long-dash and dash-dot lines: N assimilation from ammonium. Insets in d–f: same simulations on shorter PPFD scales to show trends at low PPFD. R_c and A did not vary noticeably for PPFDs above those shown here.

100 Pa) and O (2, 21 and 40 kPa), each for two values of p_e (1.5 and 1.286). For $p_e = 1.5$, neither increased f_m , decreased c_i or increased O relative to the default values given in Table 3 had any significant effect on the relationship between R_c and PPFD in young leaves. In contrast, changes in the opposite direction caused R_c to increase with PPFD between 20 and 120 $\mu\text{mol m}^{-2} \text{s}^{-1}$. At low O_2 (2%) and low f_m (0), R_c subsequently declined to its minimum (maximally suppressed) value at about 150 $\mu\text{mol m}^{-2} \text{s}^{-1}$, whereas for high c_i (100 Pa), R_c remained elevated at high PPFD, relative to its maximally suppressed value. At low p_e (1.286), however, the increase in R_c at low PPFD was evident at all

values of f_m , O and c_i , and the effect was much larger at low f_m and O and high c_i . In fact, at $c_i = 100$ Pa, R_c was increased at high PPFD even relative to its value in darkness. Similar effects were predicted for mature exporting and non-exporting leaves (not shown).

The role of p_e and the strong dependence on PPFD of the predicted effect of photorespiratory NADH on inhibition of R_c , suggests that the effect involves photosynthetic adenylate balance. In the model, limited ADP supply (ATP demand) constrains the capacity of thylakoids to dissipate excess light energy by exporting NADPH. This also influences the degree to which ATP generation via

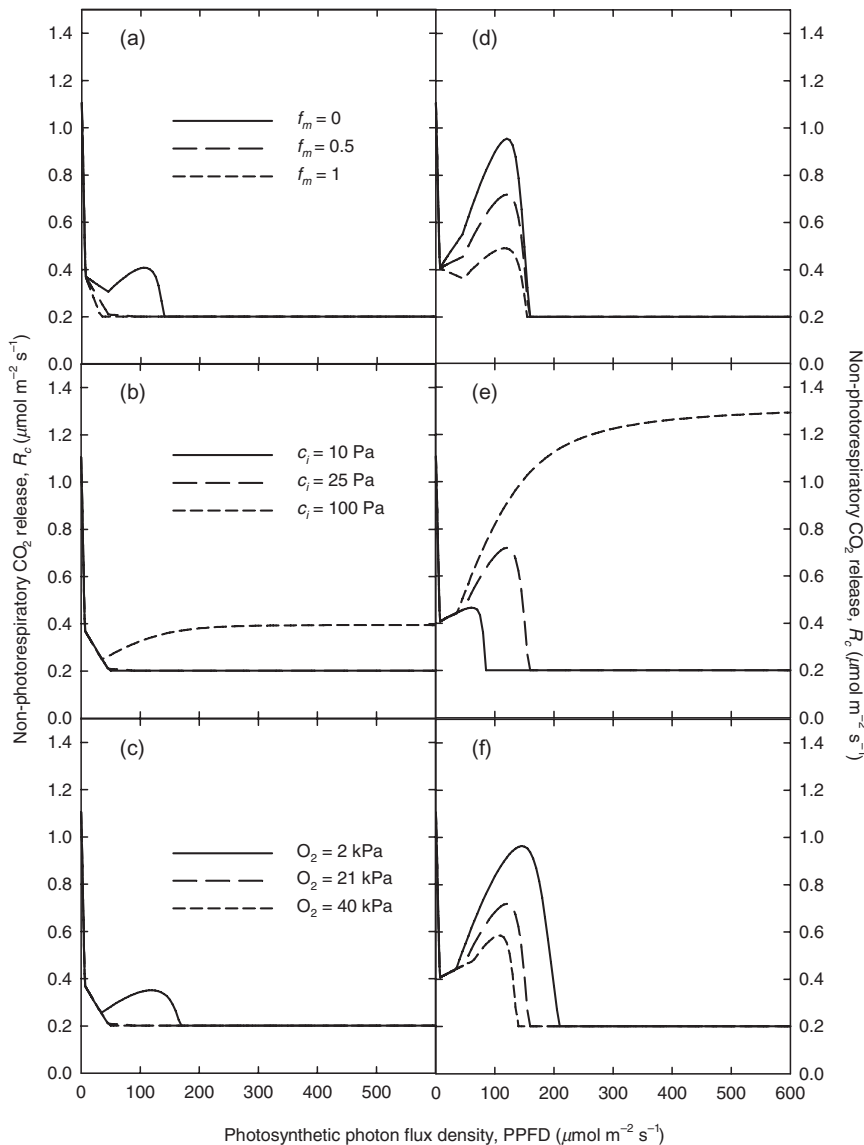


Figure 4. Effect of photorespiration on light suppression of respiration. R_c versus PPFD for different values of parameters related to photorespiration. (a, d) f_m , the fraction of photorespiratory NADH that remains in mitochondria, varied from zero to unity; (b, e) c_i , the intercellular CO₂ mole fraction, varied from 10 to 250 Pa; (c, f) oxygen concentration varied from 2 to 40%. Panels (a–c) and (d–f) show simulations at two different values of p_e , the ATP : 2e⁻ ratio for photophosphorylation (a–c: $p_e = 1.5$; d–f: $p_e = 1.286$). In all simulations, anabolic demands were assumed equal in the light and dark, stoichiometries were calculated based on N assimilation from nitrate, and simulations used demand vectors for young leaves given in Table 2. Other parameters were as shown in Table 3.

catabolic substrate oxidation (V_{cat}) is suppressed by flux-balance.

Figure 5 shows the underlying dynamics of cellular adenylate balance (net photosynthetic ATP yield, mitochondrial ATP yield and ATP demand not arising from the Calvin cycle or photorespiration), for different values of p_e and c_i . At normal c_i (25 Pa) and high p_e (1.5), net yield of ATP from photosynthesis is always non-negative, and rapidly reaches the maximum value allowed by flux balance, which is equal to non-photosynthetic ATP demand (Fig. 5a). For low p_e (1.286), net ATP yield of photosynthesis is negative under light-limited conditions (Fig. 5b). However, photoreductant export to drive oxidative phosphorylation in mitochondria cannot make up for this deficit, because there is no excess photoreductant under light-limited conditions. The balance must come instead from catabolic substrate oxidation. Therefore, the model predicts a large enhancement (rather than suppression) of R_c under light-limited conditions if p_e is low (e.g. at high c_i ; Fig. 4e).

To summarize, the effects of CO₂, O₂, photorespiratory NADH retention in mitochondria and photoreductant export on the PPFD dependence of R_c in the model are primarily driven by effects of PPFD on photosynthetic adenylate balance.

Role of changes in anabolic demands and OPPP activity in the light

As shown by Table 4 and Figs 2–4, the partitioning of anabolic demands between light and dark periods has a large influence on predicted effects of light on R_c . When biosynthetic rates are assumed to increase fourfold at the dark-to-light transition, R_c is predicted to increase sharply before being suppressed at higher PPFD by the light-related reductant flows (discussed above, see insets in Fig. 3d–f). However, in the opposite limiting case, where anabolic demands are equal in the light and dark, our model reproduces the Kok effect – an apparently discrete drop in the

Table 3. Model parameters and variables that do not depend explicitly on anabolic demand

Parameter or variable	Symbol	Value or equation	Units
Net CO ₂ assimilation rate	A	Eqn A20	$\mu\text{mol CO}_2 \text{ m}^{-2} \text{ s}^{-1}$
Net O ₂ release rate	A_o	Eqn A21	$\mu\text{mol O}_2 \text{ m}^{-2} \text{ s}^{-1}$
Intercellular CO ₂ partial pressure	c_i	25	Pa
Ratio of V_o to V_c	ϕ	$0.21(O/K_o)/(c_i/K_c)$	O ₂ /CO ₂
Product of absorbance and max quantum yield	f	0.3	e ⁻ /hν
Fraction of photorespiratory NADH that stays in mitochondria	f_m	0.5	dimensionless
Fraction of excess thylakoid redox potential dissipated as NADPH export	f_x	Eqn A9	dimensionless
Potential electron transport rate	J	$\theta_p J^2 - (J_m + fI) + fJ_m I = 0$	$\mu\text{mol e}^- \text{ m}^{-2} \text{ s}^{-1}$
Actual electron transport rate	J_a	Eqn A5	$\mu\text{mol e}^- \text{ m}^{-2} \text{ s}^{-1}$
Maximum potential electron transport rate	J_m	$2.1 \cdot V_m$	$\mu\text{mol e}^- \text{ m}^{-2} \text{ s}^{-1}$
Michaelis constant for carboxylation	K_c	40.49 ⁽¹⁾	Pa
Michaelis constant for oxygenation	K_o	27.84 ⁽¹⁾	kPa
Ambient oxygen partial pressure	O	21	kPa
ATP yield per 2e ⁻ in thylakoid ETC	p_e	1.5	ATP/2e ⁻
Actual P : O ratio	p_o	Eqn A17	ATP/O
Maximum P : O ratio	p_{om}	Eqn A8	ATP/O
Non-photorespiratory CO ₂ release rate	R_c	Eqn A11	$\mu\text{mol CO}_2 \text{ m}^{-2} \text{ s}^{-1}$
Mitochondrial O ₂ reduction rate	R_o	Eqn A16	$\mu\text{mol O}_2 \text{ m}^{-2} \text{ s}^{-1}$
Carbohydrate storage and export rate	S	$V_c - 0.5V_o - V_{ana}$	$\mu\text{mol CO}_2 \text{ m}^{-2} \text{ s}^{-1}$
ATP cost per C for storing or accessing stored carbohydrate	t	1/6 if $S > 0$; -1/3 if $S \geq 0$	ATP/C
RuBP carboxylation rate	V_c	Eqns A18 and A19	$\mu\text{mol CO}_2 \text{ m}^{-2} \text{ s}^{-1}$
Rate of carbon flow dedicated to catabolic substrate oxidation	V_{cat}	Eqns A13–A15	$\mu\text{mol CO}_2 \text{ m}^{-2} \text{ s}^{-1}$
Maximum carboxylation rate	V_m	23.78	$\mu\text{mol CO}_2 \text{ m}^{-2} \text{ s}^{-1}$
RuBP oxygenation rate	V_o	ϕV_c	$\mu\text{mol O}_2 \text{ m}^{-2} \text{ s}^{-1}$
Rate of carbon flow through OPPP to CO ₂	V_{opp}	Eqn A3	$\mu\text{mol CO}_2 \text{ m}^{-2} \text{ s}^{-1}$
Rate of NADPH export by chloroplasts	V_{px}	Eqn A4	$\mu\text{mol NADPH m}^{-2} \text{ s}^{-1}$

Simulations shown in this paper used the parameter values above unless otherwise noted in the text. K_c and K_o values are at 25 °C. Calculation of ϕ assumes the ratio of Rubisco turnover numbers for oxygenase and carboxylase is 0.21 (Farquhar *et al.* 1980). (1) (Bernacchi *et al.* 2001).

quantum yield of CO₂ (QY) at low light (e.g. Figs 3d,e & 6). This prediction arises from our hypothesis that OPPP activity is progressively inhibited by the PPFD-driven increase in thylakoid reducing power, until thylakoids can satisfy anabolic reductant demands. For example, the model predicts that QY declines by half at approximately $7 \mu\text{E m}^{-2} \text{ s}^{-1}$ for young leaves, $5 \mu\text{E m}^{-2} \text{ s}^{-1}$ for mature exporting leaves and $3 \mu\text{E m}^{-2} \text{ s}^{-1}$ in mature non-exporting leaves (Fig. 6). This mechanism for the Kok effect requires that anabolic reductant demand does not increase substantially within this range of very low PPFD. We simulated a gradual stimulation of anabolic reductant demand in young leaves by assuming B_p in darkness was one-fourth of the value in full light, and that B_p responded hyperbolically to PPFD with a 'Michaelis constant' of $50 \mu\text{E m}^{-2} \text{ s}^{-1}$: $\{B_p \text{ in light}\} = \{B_p \text{ in dark}\} \cdot \{1 + 3 \cdot \text{PPFD}/(50 + \text{PPFD})\}$. This produces a 150% stimulation at $50 \mu\text{E m}^{-2} \text{ s}^{-1}$ and a 300% stimulation at saturating PPFD. A Kok effect is still clearly evident in this simulation (dash-dot line in Fig. 6), suggesting our proposed mechanism for the Kok effect is consistent with a strong stimulation of anabolic reductant demand at low light.

The potential contribution of suppressed CO₂ release from the chloroplast OPPP to the inhibition of R_c by light can be quantified as the ratio of V_{opp} to R_c in the dark, for leaves with equal anabolic demands in darkness and light. These values range from 0.19 to 0.49 (19 to 49%) for the range of conditions used in the simulations shown in Table 4

and Fig. 4; they are smallest in mature/non-exporting leaves fed NH₄⁺ and largest in mature/exporting leaves fed NO₃⁻.

Role of carbohydrate sourcing, export and storage

Metabolic carbon demands in the light are assumed to rely on recently fixed TP as much as possible, because of the ATP costs of storing or exporting TP as sucrose or starch. Increasing photosynthetic TP output at low PPFD therefore reduces ATP demand. However, when TP supply exceeds anabolic demand for carbohydrate, the excess must be stored or exported, increasing ATP demand. The net effects on ATP demand are illustrated by short-dashed lines in Fig. 5, which show changes in non-photosynthetic ATP demand with PPFD. Biosynthetic and maintenance demands are constant with PPFD, and the effect of TP use and storage is the decline up to about $50 \mu\text{mol m}^{-2} \text{ s}^{-1}$ (at $c_i = 25 \text{ Pa}$), followed by a more gradual and saturating increase. Storage/export costs contribute approximately 25% of total non-photosynthetic ATP demands at high light in these simulations for young leaves, and about 37% for mature non-exporting leaves (not shown). However, excluding these storage/access costs has no effect on R_c at high light, because catabolic substrate oxidation is inhibited and there is plenty of ATP available from photosynthesis. In fact, this helps relieve inhibition of R_c at high light by 1–4%

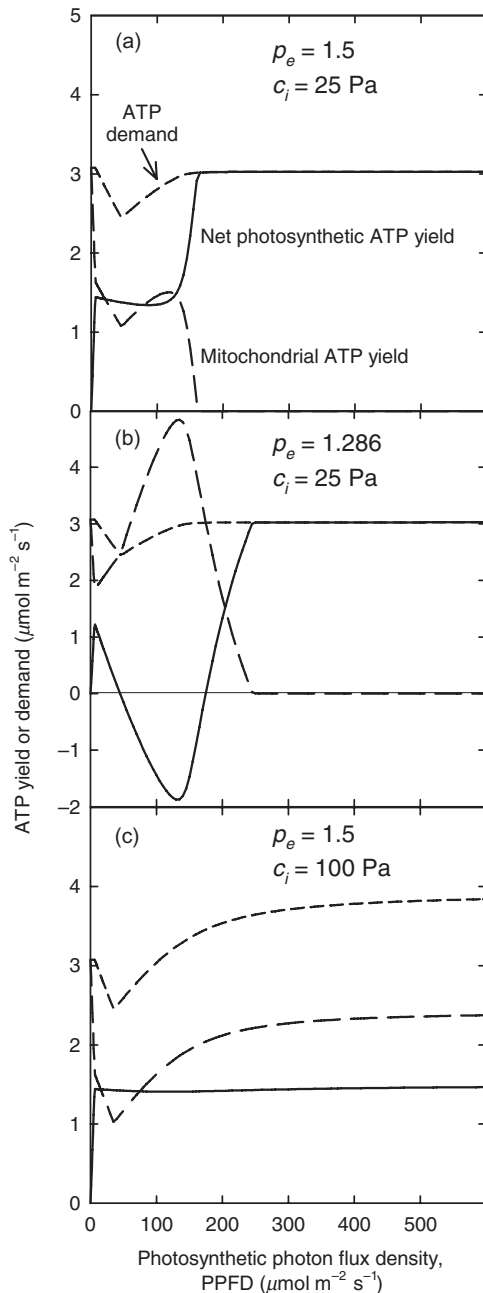


Figure 5. Effect of light on adenylate balance. Effect of variation in PPFD on components of cellular adenylate balance in the model: net photosynthetic ATP yield [calculated as $0.5p_e J_a - (3 + 3.5\phi) \cdot V_c$]; mitochondrial ATP yield [$2p_o R_o + p_e V_{cat}$]; and non-photosynthetic ATP demand [$B_t + M + tS$]. Symbols are defined in Table 3. Simulations were performed for three different combinations of values of two parameters that influence adenylate balance: p_e , the ATP : $2e^-$ ratio for photophosphorylation, and c_i , the intercellular CO_2 partial pressure. (a) $p_e = 1.5$, $c_i = 25$ Pa; (b) $p_e = 1.286$, $c_i = 25$ Pa; (c) $p_e = 1.5$, $c_i = 100$ Pa. Anabolic demands were assumed equal in the light and dark, stoichiometries were calculated based on N assimilation from nitrate, and simulations used demand vectors for young leaves in Table 2. Other parameters were as shown in Table 3.

(more in young leaves, less in mature leaves) because those costs contribute to R_c in the dark. However, if nocturnal starch breakdown were augmented in our model such that included anabolic demands were augmented by export demands equal to the rate of storage/export (S) at high light (that are not currently included), then total nocturnal ATP demand would be increased by a factor of 3–4 in young leaves. Thus, storage/export costs may contribute ~5–15% to suppression of R_c in the light. Proper treatment of this question may require dynamic simulation of starch pools.

Predicted dynamics of P : O ratio and engagement of alternative electron sinks

The model predicts that catabolic substrate oxidation, V_{cat} , declines to zero in the light in many cases, due to availability of reductant or ATP from other sources. When those sources continue to increase even after V_{cat} is fully inhibited, ATP supply will exceed demand unless the P : O ratio (p_o) for oxidative phosphorylation is reduced to less than its theoretical maximum value (p_{om}).

Flux-balance thus requires engagement of one or more of several mechanisms to reduce proton transport relative to electron flow in the mETC: oxidation of NADH at dehydrogenases other than Complex I (the latter leads to the transport of four more protons than other dehydrogenases), alternative oxidase or uncoupling protein. Additionally, adenylate flux balance places an upper limit on photoreductant export, because whole-chain thylakoid electron transport is inextricably coupled to photophosphorylation. This limits the fraction (f_x) of excess thylakoid reducing potential that can be dissipated by NADPH export. Figure 7 shows the model's predictions for p_o , p_{om} and f_x for young leaves. The model predicts that p_o remains at p_{om} when photosynthesis is light-limited, but that p_o declines to zero during the transition to carboxylation limitation. This is required because excess photoreductant and ATP supply from photosynthesis require a steep decline in mitochondrial ATP yield to maintain flux balance. At higher light, f_x is constrained to decline with increasing PPFD as well, reaching 0.16 at $1000 \mu mol m^{-2} s^{-1}$. At low p_e (Fig. 7b), these trends are qualitatively similar, but the curves are all shifted to higher PPFD, due to reduced ATP yield from photosynthesis. At $c_i = 100$ Pa (Fig. 7c), leaves are never carboxylation-limited, so p_o remains at p_{om} and f_x remains at 1.0 for all PPFDs. Simulations of p_o , p_{om} and f_x for mature exporting leaves and mature non-exporting leaves were nearly identical to those for young leaves (not shown). Changing from NO_3^- to NH_4^+ supply shifted curves slightly to the right when $p_e = 1.5$, but had the opposite effect when $p_e = 1.286$ (not shown).

Sensitivity to anabolic supply/demand parameters

We assessed model sensitivity to variations in the parameters describing anabolic and maintenance demands (V_{ana} , V_{by} , B_t ,

Table 4. Model predictions for respiratory CO₂ release (R_c , $\mu\text{mol m}^{-2} \text{s}^{-1}$) and O₂ consumption (R_o , $\mu\text{mol m}^{-2} \text{s}^{-1}$) in the dark and light, net CO₂ assimilation (A , $\mu\text{mol m}^{-2} \text{s}^{-1}$) in the light, ratio of net CO₂ to O₂ exchange in the dark and light (RQ and AQ, respectively), and inhibition of respiration in high light [% inhib, $100 \cdot [1 - R_c(\text{light})/R_c(\text{dark})]$]

Leaf	Dark ana.	N	R_c (dk)	R_o (dk)	RQ	R_c (lt)	R_o (lt)	AQ	A (lt)	% inhib
Y	high	NO ₃ ⁻	1.11	0.56	1.98	0.20	0.93	0.90	5.18	81.8
Y	low	NO ₃ ⁻	0.57	0.35	1.63	0.32	0.91	0.85	5.06	43.1
Y	high	NH ₄ ⁺	0.75	0.57	1.31	0.20	1.30	0.97	5.18	73.1
Y	low	NH ₄ ⁺	0.42	0.35	1.20	0.32	1.50	0.95	5.06	23.9
MX	high	NO ₃ ⁻	0.55	0.31	1.80	0.06	0.83	0.96	5.33	90.0
MX	low	NO ₃ ⁻	0.35	0.25	1.40	0.09	0.76	0.93	5.30	74.3
MX	high	NH ₄ ⁺	0.32	0.31	1.03	0.06	1.07	1.00	5.33	82.8
MX	low	NH ₄ ⁺	0.25	0.25	1.02	0.09	1.14	1.00	5.30	64.9
M	high	NO ₃ ⁻	0.42	0.28	1.51	0.06	0.93	0.97	5.33	86.0
M	low	NO ₃ ⁻	0.29	0.24	1.24	0.09	0.92	0.96	5.29	67.7
M	high	NH ₄ ⁺	0.32	0.28	1.14	0.06	1.03	0.99	5.33	81.7
M	low	NH ₄ ⁺	0.25	0.24	1.07	0.09	1.08	0.99	5.29	62.6

Under *leaf*, Y, MX and M refer to simulations that used anabolic demand terms for young, mature-exporting and mature non-exporting leaves, respectively, as given in Table 2. Under *dark ana.* (dark anabolism), *high* refers to simulations assuming equal anabolic rates in the dark and in the light, and *low* refers to simulations assuming fourfold higher anabolic rates in the light, with absolute demands adjusted to conserve total diel output for a 12-hr light period. *N* refers to nitrogen supply (nitrate vs. ammonium) assumed for amino acid biosynthetic stoichiometries. Predictions used parameter values given in Tables 2 and 3. Values in the light are at a photosynthetic photon flux density of $1000 \mu\text{mol m}^{-2} \text{s}^{-1}$.

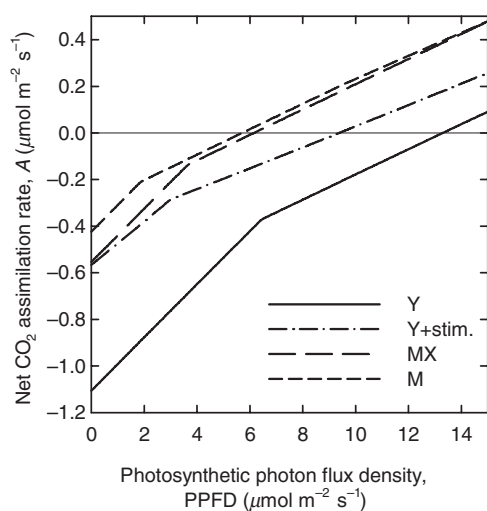
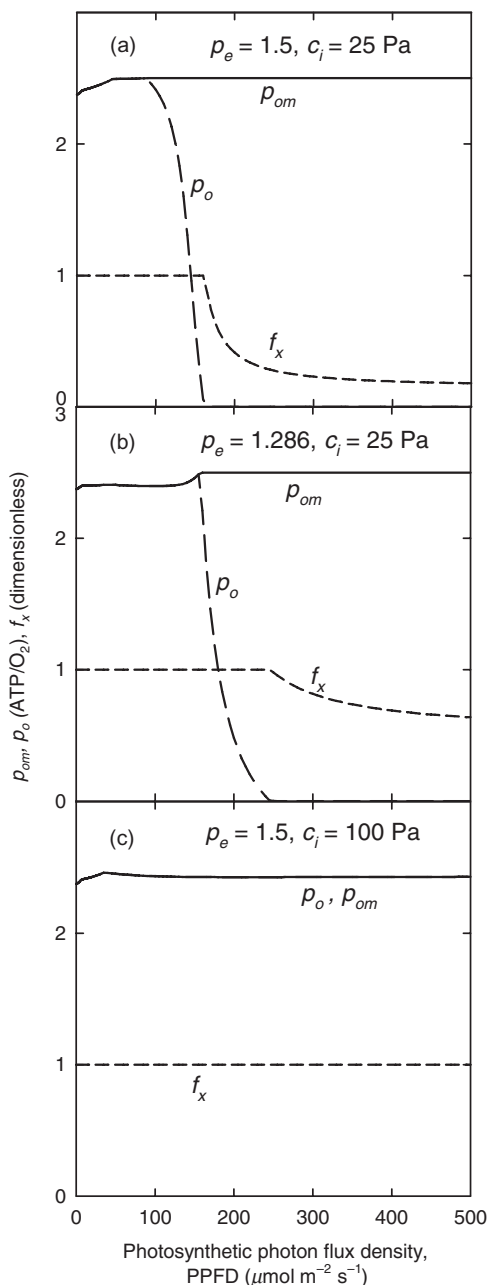


Figure 6. Effect of anabolic demand on apparent Kok effect. Relationship between net CO₂ assimilation rate (A) and PPFD at very low light, showing an apparent Kok effect (discrete decline in quantum yield of A at low PPFD). Simulations were repeated under four different sets of assumptions governing anabolic demands. Three of these assumed that anabolic demands were equal in the light and dark: (solid line, Y), young leaves. (long-dash line, MX), mature leaves synthesising amino acids for export. (short-dash line, M), mature leaves not synthesising amino acids for export. The fourth simulation, represented by the dash-dot line and symbolized 'Y + stim', used anabolic demands for young leaves but further assumed that anabolic demand is progressively enhanced by PPFD, such that demand increases by 150% at a PPFD of $50 \mu\text{mol m}^{-2} \text{s}^{-1}$ as compared to darkness. In the model, the Kok effect is caused by a progressive suppression of oxidative pentose phosphate pathway activity in proportion to increasing thylakoid reducing power. In all simulations, stoichiometries were calculated based on N assimilation from nitrate.

M , B_n and B_p) by measuring elasticity of output variables with respect to these parameters [elasticity of y with respect to x is the relative change in y observed in response to a relative change in x ; i.e. $(\delta y/y)/(\delta x/x)$ or $\partial \ln y / \partial \ln x$].

Four output variables were used (Table 5): R_c in the dark, R_c at $1000 \mu\text{mol m}^{-2} \text{s}^{-1}$, proportional inhibition at $1000 \mu\text{mol m}^{-2} \text{s}^{-1}$ and the PPFD at which catabolic substrate oxidation was fully inhibited. These calculations used simulations for young leaves under nitrate supply, with equal anabolic demands during day and night. The value of R_c at saturating light was insensitive to all supply/demand parameters except V_{by} (CO₂ efflux as a by-product of anabolic carbon flow), for which the elasticity of R_c was 1. As a result, inhibition was also most sensitive to V_{by} (elasticity = -0.18). Among other parameters, chloroplastic NADPH demand (B_p) had the strongest effects on R_c in the dark and on % inhibition (elasticities of 0.43 and 0.10, respectively), followed by biosynthetic ATP demand (B_t) (elasticities of 0.20 and 0.05, respectively). NADPH demand also had the strongest effect on threshold PPFD for non-phosphorylating electron flow in the mETC (elasticity = -6.92); net anabolic NADH generation had a similar but smaller effect (-3.00), whereas B_t had a strong effect in the opposite direction (+4.79).

These results suggest that changes in leaf composition and/or metabolic demands that increase ATP demand, such as increased protein, polysaccharide or phenolic synthesis, or decreased fatty acid or terpenoid synthesis, will reduce the need for engagement of alternative oxidase and uncoupling protein. Conversely, changes that increase net anabolic NADH yield or NADPH demand relative to ATP demand, most notably including increased fatty acid or terpenoid synthesis, will enhance AOX requirements.



DISCUSSION

Our model predicts highly variable suppression of R_c in high light, ranging from 24 to 90%. Consistent with these predictions, measured inhibition of R_c in the light varies widely. For example, 85% inhibition has been recorded for *Spinacia oleracea* L. (Brooks & Farquhar 1985), 30–70% inhibition for mature *Eucalyptus pauciflora* Sieb. ex Spreng. (Atkin *et al.* 2000), 3–39% inhibition for 4-month-old *E. pauciflora* (Kirschbaum 1984), 43–72% inhibition for *Nicotiana tabacum* L. leaves at low irradiance ($140 \mu\text{E m}^{-2} \text{s}^{-1}$) (Atkin, Evans & Siebke 1998), 36% for young leaves and 81% inhibition for mature leaves of *Heteromeles arbutifolia* and 62% inhibition for medium-aged leaves of *Lepechinia*

Figure 7. Effect of light on mitochondrial P : O ratio and photoreductant export. Conditions influencing the engagement of alternative oxidase (AOX) or other non-phosphorylating pathways in mitochondrial electron transport were probed by simulating effects of light on the maximum and actual P : O ratio (p_{om} and p_o , respectively; solid and long-dash lines) and on the fraction of excess thylakoid reducing potential dissipated via NADPH export (f_x , short-dash line). Reduction of p_o below p_{om} implies engagement of non-phosphorylating pathways; similarly, reduction of f_x below 1 implies a reduced capacity of mitochondria to act as electron sinks for excess photoreductant. These simulations were repeated at high and low p_e and c_i , as in Fig. 5, to assess the effect of photosynthetic adenylate balance on AOX engagement: (a) $p_e = 1.5$, $c_i = 25$ Pa; (b) $p_e = 1.286$, $c_i = 25$ Pa; (c) $p_e = 1.5$, $c_i = 100$ Pa. Anabolic demands were assumed equal in the light and dark, stoichiometries were calculated based on N assimilation from nitrate, and simulations used demand vectors for young leaves in Table 2. Other parameters were as shown in Table 3.

fragrans (Villar *et al.* 1995). Below, we discuss various explanations for these phenomena in relation to our model.

The role of variation in anabolic demands

In our model, the most important factor in explaining this variability is variation in anabolic demands, both among leaves in differing stages of development and between light and dark conditions. For example, the model predicts greater inhibition in mature leaves (65–90%) than in young leaves (35–82%), consistent with the data of Villar *et al.* (1995). In our model, this effect can be traced to two factors. First, mature leaves have smaller anabolic demands for reductant. At high light, excess photoreductant exported to the cytosol as NADH offsets the NADH yield from glycolysis and the TCA cycle; therefore, in order to maintain flux

Table 5. Elasticities of model outputs with respect to anabolic and maintenance supply/demand parameters, calculated as the % change in the model output given in the first row in response to a 1% increase in the anabolic supply/demand parameter given in the left column

	R_c (dark)	R_c (light)	% inhib	AOX PPFD
V_{ana}	0.10	0.00	0.02	-1.33
V_{by}	0.18	1.00	-0.18	0.00
B_t	0.20	0.00	0.05	4.79
M	0.19	0.00	0.04	4.39
B_n	-0.11	0.00	-0.02	-3.00
B_p	0.43	0.00	0.10	-6.92

Parameters in the left column are defined in Table 2.

Model outputs: R_c (dark): R_c in the dark; R_c (light): R_c at PPFD = $1000 \mu\text{E m}^{-2} \text{s}^{-1}$; % inhib: % inhibition of R_c at $1000 \mu\text{E m}^{-2} \text{s}^{-1}$; AOX PPFD: PPFD at which catabolic substrate oxidation is fully suppressed, requiring engagement of non-phosphorylating pathways such as alternative oxidase (AOX) to maintain electron flow for NADH flux balance. Simulations were for young leaves with N supplied as nitrate; all other parameters as given in Tables 2 and 3.

balance for NADH, mature leaves in high light must have a lower rate of catabolic substrate oxidation, and therefore less CO₂ release. By contrast, young leaves consume more of this excess photoreductant in anabolic processes – relieving some of the potential suppression of R_c . Second, anabolic carbon flow also releases CO₂ as a by-product, and that CO₂ release (V_{by} in our model) is a much larger fraction of R_c in the dark for young leaves because of their greater anabolic carbon flow. Since V_{by} is not subject to suppression by PPFD, the fraction of R_c subject to inhibition by light is smaller in young leaves. For example, our model predicts greater inhibition of R_c when anabolic carbon flow is equal in the light and in the dark (73–90%) than when anabolism is assumed to be up-regulated in the light by a factor of four (24–74% suppression of R_c).

It is difficult to generalize about diel variation in anabolic demands. One component, in particular nitrate assimilation, is a major sink for reductant in the light (Bloom *et al.* 1989), and nitrate reductase activity is strongly enhanced by light both at the transcriptional and translational levels (Kaiser, Weiner & Huber 1999; Sheremeti *et al.* 2002; Stitt *et al.* 2002). Nitrogen assimilation is also suppressed by a reduction in carbohydrate status (Fritz *et al.* 2006), and therefore by the duration of the dark period. Nevertheless, nitrate reduction often continues in the dark, albeit often at reduced rates (9–76% of diurnal rates in a range of species [Reed *et al.* 1983]; ~50% [Aslam *et al.* 1979] or 88% [Bloom *et al.* 1989] in *Hordeum vulgare* L.). In species that perform little or no nitrate reduction in leaves, amino acid synthesis in leaves does not, in principle, require light. Additionally, Fritz *et al.* (2006) found that glutamate levels were conserved over the diel cycle and aspartate synthesis was increased in the dark relative to the light in tobacco. Some of the citrate required for glutamate synthesis is generated in the dark and stored in vacuoles (Scheible, Krapp & Stitt 2000; Urbanczyk-Wochniak *et al.* 2005), which may contribute to the temporal stability of glutamate concentrations (Tcherkez & Hodges 2008). These observations could be applied to our model by separating these steps before calculating anabolic demand terms, which would shift significant NADH and ATP yield (arising from C flow to citrate) from the light to the dark – as well as possibly decreasing R_c in the dark and enhancing it in the light. The model's predictions about mitochondrial oxygen consumption (R_o) are also sensitive to N assimilation. For example, lesser R_o and greater RQ are predicted for nitrate than ammonium nutrition (Table 4). This is consistent with data of Bloom *et al.* (1989) on *H. vulgare*, and it reflects the diversion of reductant from the mETC to NO₃⁻ reduction. The recent emergence of high resolution differential oxygen analysers (e.g. Willms *et al.* 1997; Kruse & Adams 2008) makes it possible to begin investigating these processes more widely.

Potential suppression of R_c in the light may also be related to other aspects of leaf gas exchange, including nocturnal transpiration and net diurnal carbon gain. For example, nitrogen assimilation is strongly influenced by N supply (Stitt *et al.* 2002; Fritz *et al.* 2006) and can be influenced by the rate of N delivery in the transpiration

stream (McDonald, Erickson & Kruger 2002) suggesting that nocturnal respiration linked to N assimilation may be associated with nocturnal transpiration. This is consistent with the hypothesis that nutrient delivery is an important function of nocturnal transpiration (McDonald *et al.* 2002; Caird, Richards & Donovan 2007). Additionally, there is evidence that nocturnal transpiration scales with total photosynthetic carbon gain during the previous day (Easlon & Richards 2009), leading to a hypothesis that nocturnal transpiration is regulated to match nitrogen delivery with supply of respiratory substrates.

Other evidence points to a link between diurnal carbon gain and nocturnal respiration (and therefore potential % suppression of R_c in the light). Steady-state respiratory CO₂ release in the dark is typically correlated with sucrose concentrations (e.g. Gessler *et al.* 2007) and is greater after a period of illumination than after an extended period of darkness, both of which have been taken as evidence of dependence on carbohydrate concentrations (Azcón-Bieto & Osmond 1983; Atkin *et al.* 1997). This may result at least partly from the ATP costs of sucrose export. It is well established that carbohydrate metabolism in leaves tends to be regulated such that sucrose export from source leaves is relatively stable over a diel cycle (Buchanan, Gruissem & Jones 2000). Although our model implicitly includes nocturnal starch degradation for anabolic carbon flow (production of C skeletons), it does not include nocturnal export *per se*. Adding nocturnal ATP export costs equivalent to predicted export rates under high light conditions enhances R_c by ~10% in the dark (not shown), suggesting that nocturnal carbohydrate metabolism for export may play a significant, if not dominant, role in suppression of R_c in the light in source leaves. Experiments to measure suppression should control for variations in diurnal carbon gain in the days before and during respiration measurements.

Another feature of our model – the Kok effect – is also sensitive to variation in anabolic demands with PPFD. The model reproduces the Kok effect by assuming that OPPP activity is progressively suppressed in very low light, as photoreductant supply increases. This hypothesis is supported by data from *Chlamydomonas reinhardtii*, a single-cell alga (Farr, Huppe & Turpin 1994), showing inhibition of chloroplastic G6PDH in very low light (5–30 $\mu\text{mol m}^{-2} \text{s}^{-1}$). It is also consistent with findings that photorespiration is not centrally involved in the Kok effect (Kirschbaum 1984; Sharp *et al.* 1984). This hypothesis requires that, if anabolic demands are enhanced by light, enhancement is much weaker than inhibition of chloroplastic G6PDH at low light. Our simulations suggest that a doubling of anabolic demand between 0 and 50 $\mu\text{mol m}^{-2} \text{s}^{-1}$ PPFD does not eliminate a substantial Kok effect in young leaves with strong anabolic demands (Fig. 6). These predictions again highlight the need to better characterize variation in anabolic carbon flow with PPFD, especially in very low light. Our hypothesis regarding the cause of the Kok effect also suggests that its magnitude should scale with anabolic demands in the dark, because those demands determine

rates of CO₂ release from the OPPP in the dark. This is consistent with data showing the Kok effect scales with rates of dark respiration (Sharp *et al.* 1984), although it is unclear whether variation in dark R_c in those experiments resulted from differences in anabolism. We emphasize that the Kok effect arises in our model from a hypothesis about the regulation of the OPPP with respect to thylakoid e⁻ transport, and that the model's phenomenological similarity to real leaves does not prove the hypothesis.

The role of direct interactions with photosynthesis and photorespiration

The model suggests that mitochondrial function is often required to oxidize excess photoreductant. Most available data are consistent with this prediction (Saradadevi & Raghavendra 1992; Raghavendra, Padmasree & Saradadevi 1994; Hurry *et al.* 1995). Oligomycin, which inhibits mitochondrial electron flow by blocking the dissipation of proton gradient through ATPase, reduces photosynthetic rates at even moderate irradiances (mesophyll protoplasts of barley, Krömer & Heldt 1991a; mesophyll protoplasts of pea, Saradadevi & Raghavendra 1992; e.g. leaves of rye, Hurry *et al.* 1996). The latter authors reported increased photoinhibition under very high light for leaves treated with a range of mitochondrial electron transport inhibitors, including oligomycin (Saradadevi & Raghavendra 1992). That different inhibitors produce similar effects argues against artefacts as results of side effects of inhibitors. Photoinhibition also involves ATP-dependent repair of reaction-centre D1 protein (Krause 1988; Greer, Ottander & Öquist 1991). This is not explicitly included in our model, albeit that additional ATP demand would enhance capacity for photoreductant export, and thus act as a negative feedback on photoinhibition. Enhanced photoinhibition in CO₂-limited conditions, such as when c_i is limited by reduced leaf conductance in low humidity or drought, is due partly to reduced ability of carboxylation to consume photoreductant (Epron 1997). Our model is consistent with this observation as well, because increasing c_i reduces both photoreductant export and suppression of R_c in the model (Figs 4b & 5).

Reduced c_i enhances photorespiration and thus NADH production from Gly decarboxylation in mitochondria. The NADH thus produced can contribute electrons to the mETC, provided a fraction (f_m) of it is not transported to peroxisomes for hydroxypyruvate reduction but instead remains in mitochondria. Raghavendra, Reumann & Heldt (1998) demonstrated the feasibility of NADH transport to peroxisomes, and measurements suggest that 25–50% of photorespiratory NADH is exported (Krömer & Heldt 1991b; Hanning & Heldt 1993). This gives $f_m = 0.5$ – 0.75 (cf. our default value of 0.5). Reduction in f_m below this value substantially relieves inhibition of R_c (Fig. 4a), but only to the extent that photosynthesis is light-limited. Excess photoreductant is available under light-saturated conditions, so exported photorespiratory NADH simply 'redirects' (in a flux-balance sense) those photosynthetically derived

electrons from hydroxypyruvate reduction to the mETC. The model predicts therefore that reduced c_i can enhance suppression of R_c at all irradiances, but more so at low to intermediate irradiances, due to the involvement of photorespiratory NADH.

The relationship between photorespiration and non-photorespiratory CO₂ release was recently investigated in labelling experiments by Tcherkez and colleagues (Tcherkez *et al.* 2008). They found that photorespiratory conditions increased decarboxylation of labelled pyruvate fed to cocklebur (*Xanthium strumarium* L.) leaves. The authors interpreted their results as evidence of enhanced TCA cycle activity to generate α -ketoglutarate for glutamate synthesis, to support faster photorespiratory glycine–serine cycling. As discussed above, our model predicts the opposite: enhanced photorespiration should suppress non-photorespiratory decarboxylation, because of the increased supply of NADH in the mitochondrial matrix. The discrepancy may result partly from our model's flux balance premise: photorespiration generates no *net* Glu demand, nor therefore any enhancement of *steady-state* TCA carbon flow. However, the transient increase in CO₂ release resulting from Glu synthesis to increase Glu pool size should be on the order of 120 $\mu\text{mol m}^{-2}$ at most [this assumes a leaf Glu content of 3.0 $\mu\text{mol g}^{-1}$ fresh wt, the maximum value reported by Tcherkez *et al.* (2008); a net release of one CO₂ molecule per Glu synthesized, which assumes OAA is regenerated by carboxylation of PEP; and a specific leaf area of 0.04 $\text{m}^2 \text{g}^{-1}$, reported by Anten & Hirose (1998) for the congener *Xanthium canadense*]. This corresponds to 20 min of enhanced CO₂ release at the reported level ($\sim +0.1 \mu\text{mol m}^{-2} \text{s}^{-1}$). It is possible that pool sizes of other TCA cycle intermediates also require enhancement to support higher rates of photorespiratory metabolism. Nevertheless, this example demonstrates the utility of an integrative flux-balance model such as ours, both in providing an objective check against intuition when interpreting surprising results, and in providing a quantitative framework that can be transparently modified to accommodate new knowledge about metabolic interactions like those examined by Tcherkez *et al.* (2008).

Implications for non-phosphorylating electron flow

Our model predicts that a large part of carbon flow through the TCA cycle – specifically, the part that we distinguish as catabolic substrate oxidation, V_{cat} , to differentiate it from TCA activity linked to anabolism – must be suppressed in the light to maintain adenylate balance [It is important to note that this does not imply the absence of decarboxylation in pyruvate conversion or the TCA cycle: on the contrary, such carbon flow is required to supply C skeletons for anabolic activity in the light (Raghavendra & Padmasree 2003). CO₂ release associated with the latter C flow is represented by the term V_{by}]. When V_{cat} is 100% suppressed, adenylate balance requires that any further increase in electron flow to the mETC is coupled to a decline in the P : O

ratio (p_o), either by dissipation of proton gradients via uncoupling protein, or by diversion of electrons through non-phosphorylating pathways terminating at alternative oxidase. Under typical conditions for a young leaf with high anabolic demands, our model suggests that these mechanisms must begin to reduce p_o at a fairly low PPFd, at the beginning of the transition to Rubisco limitation (about $100 \mu\text{mol m}^{-2} \text{s}^{-1}$ for the parameters in Table 3). These transitions are predicted to occur at lower PPFd for low c_i , or for leaves with lower anabolic demands, whereas at high c_i (100 Pa), p_o never declines below its maximum value because photosynthesis remains light-limited (Fig. 7b). This has a variety of implications for ecological correlates of AOX utilization. It is consistent with findings that electron flow through AOX increases under water stress conditions in soybean leaves (Ribas-Carbo *et al.* 2005) and wheat leaves (Bartoli *et al.* 2005). The latter authors also found that AOX involvement enhanced photosynthetic electron transport. However, in darkened leaves of *Pinus radiata*, Kruse & Adams (2008) found greater AOX involvement in young, expanding foliage, which should have much greater anabolic demands. Our model does not predict a reduction in p_o below its 100%-COX maximum value (p_{om}) in the dark, using the anabolic demand profiles given in Table 2. However, if a biosynthetic requirement for 30% terpenoids (by dry weight) is added to simulate large NADH yield as a by-product of anabolic carbon flow through glycolysis to acetyl-CoA (the starting point for terpenoid biosynthesis), then the model does in fact predict greater AOX engagement for young than mature leaves (not shown). This effect arises because terpenoid synthesis yields a great deal of ATP and NADH, both of which must suppress catabolic substrate oxidation to maintain flux balance. More generally, our analysis of the model's sensitivity to variation in the anabolic demand/supply parameters (Table 5) indicates that variations in ATP, NADH and NADPH supply and demand have a strong effect on the threshold PPFd for AOX involvement. Together, these results emphasize that 'biochemical profiles' of plant tissues are critical determinants of AOX engagement.

The reductant demands of nitrate assimilation have a somewhat paradoxical effect on predicted non-phosphorylating electron flow. By consuming reductant that may otherwise increase mitochondrial electron flow independent of ATP demand, one may expect NO_3^- assimilation to alleviate reductions in p_o associated with photoreductant flows. Indeed, Escobar, Geisler & Rasmusson (2006) found that in *Arabidopsis thaliana*, AOX genes were up-regulated in response to NH_4^+ nutrition, but down-regulated in response to NO_3^- nutrition. Our model predicts that the effect of NH_4^+ nutrition on P : O ratio, and thus presumably on AOX activity, depends on the ATP : $2e^-$ ratio (p_e) in photosynthesis. Thylakoid electron transport for NO_2^- reduction is inextricably coupled to photophosphorylation, increasing chloroplastic ATP yield. If p_e is large, ATP supply exceeds demand, driving down the P : O ratio; if p_e is small, this effect is overridden by the effect of reductant consumption by NO_3^- assimilation on the P : O ratio. These

considerations are exemplified by the predicted effects of p_e on mitochondrial O_2 consumption (R_c) in the light in young leaves under NO_3^- nutrition: reducing p_e from 1.5 to 1.286 more than doubles R_c , from $= 0.93$ to $2.43 \mu\text{mol m}^{-2} \text{s}^{-1}$ (not shown). We conclude that the role of N nutrition in light inhibition of R_c and stimulation of non-phosphorylating pathways in mitochondria may depend critically on the actual value of p_e , and on whether a plant is grown and studied in light-limited or light-saturated conditions.

Importance of the photosynthetic ATP : $2e^-$ ratio (p_e)

The model's sensitivity to the numerical value of p_e also arose in other simulations (Figs 4, 5 & 7), highlighting this parameter's critical importance for understanding how respiration and photosynthesis interact.

Our default value of 1.5 is based on consensus values of 3 for the H^+/e^- ratio and 4 for the H^+/ATP ratio (Harau & de Kouchkovsky 1998; Heber 2002). However, the latter assumes three turns of ATPase per ATP, one H^+ per subunit per turn, and 12 subunits; Seelert *et al.* (2000) observed spinach ATPase with 14 subunits rather than 12, which would increase the H^+/ATP ratio from 4 (12/3) to 4.67 (14/3) and reduce the p_e ratio to 1.286 (18/14). Postulated cyclic or pseudo-cyclic electron transport would also increase p_e . Given the central role of adenylate balance in respiration-photosynthesis interactions in our model, we need greater clarity about the actual value of p_e . Critically, however, our model predicts that ATP yield from photosynthesis will be positive under most light-saturated conditions for either p_e value, and at all positive PPFds for $p_e = 1.5$. The latter may seem surprising, given that p_e needs to equal about 1.55 to balance ATP and NADPH requirements in the Calvin cycle and photorespiration at 21 kPa O_2 and 25 Pa c_i . There are two explanations for this. First, in the model, photoreductant is diverted to peroxisomes to compensate for the photorespiratory NADH that remains in mitochondria. Eliminating this diversion by setting $f_m = 0$ substantially reduces the net ATP yield of photosynthesis (not shown). Secondly, the photosynthetic electron flow required to satisfy anabolic demands in the light also necessarily yields ATP. When considering stoichiometric requirements of the Calvin cycle in real leaves, it may be necessary to account for these Calvin cycle-independent photoreductant sinks and ATP sources (Noctor & Foyer 1998).

Mechanisms for subcellular adenylate and reductant coupling

Our model does not specify the shuttling mechanisms by which subcellular adenylate, reductant and carbon skeleton pools are coupled to balance supply and demand at the cellular level. Potential coupling mechanisms have been discussed by numerous recent reviews on mitochondria-chloroplast interactions (Krömer 1995; Hoefnagel *et al.* 1998; Raghavendra & Padmasree 2003). Here, we discuss

them briefly to highlight how the model could be elaborated to reflect new data and understanding of transport processes. Chloroplasts can import ATP rapidly via the DHAP/3-PGA shuttle, but they have a much smaller capacity for ATP export than mitochondria (Hoefnagel *et al.* 1998). Our model does not explicitly limit ATP export *per se* from chloroplasts. However, under high light conditions, photophosphorylation is limited by demand, so the model requires chloroplasts to export ATP only under light-limited conditions, and only if the ATP : $2e^-$ ratio and the rate of anabolic consumption of photoreductant are both sufficient to yield a surplus of ATP in the Calvin cycle. Such a non-exportable surplus would reduce the sensitivity of both R_c and thylakoid electron transport to PPFD at low light. This again begs clarity around the numerical value of p_e . The model assumes that excess photoreductant is exported to the cytosol, generating NADH that reduces either O_2 (in mitochondria) or hydroxypyruvate (in peroxisomes). Chloroplasts can export reducing power via either the DHAP/3-PGA shuttle or the Mal/OAA shuttle (Krömer 1995; Hoefnagel *et al.* 1998); the former shuttles NADPH to the cytosol at the cost of one ATP, whereas the latter incurs no such cost. Our model assumes that only the Mal/OAA shuttle operates. Mitochondria can import or export redox equivalents by Mal/OAA cycling as well. It is conceivable, although we are unaware of any evidence to this effect, that the sizes of carbon pools involved in these shuttles could limit their activity. Such a limitation is most likely to arise given a large anabolic demand for carbon skeletons. Even so, a small and transient anapleurotic carbon flow could remedy any limitation of activity.

Some thoughts on the nature of our model

A natural challenge to our model, and thus to any inferences drawn from it, is that it is not based explicitly on biochemical kinetics. Here it differs from the FCB model (Farquhar *et al.* 1980). This has two implications: (1) our model cannot readily accommodate kinetic or capacity limitations on flows through various metabolic pathways nor, therefore, effects of temperature on kinetics; and (2) our model implicitly contains a broader set of assumptions than those that are explicitly stated in its development – namely that the enzyme activities and substrate and cofactor concentrations that determine the rates of every reaction sequence in leaf carbon metabolism are coordinated so as to maintain a metabolic flux-balance consistent with the imposed vector of anabolic and maintenance demands. A corollary challenge is that it may seem philosophically inconsistent to combine a kinetic model like FCB with a non-kinetic model. We offer several thoughts in support of the usefulness of our approach, as it relates to these challenges. First, FCB modelled a process that is directly limited by two measurable external resource supplies (CO_2 and light), and that is relatively linear compared to the rest of carbon metabolism. In comparison, respiratory metabolism in leaves is so highly complex and so high-dimensional that a rigorous, integrated kinetic model is such a challenge that

it will likely remain elusive for some years to come. An analytical kinetic model may never be possible. Secondly, FCB is also partly based on flux balance, via the assumptions of constant total pyridine nucleotide pool size $[(NADPH) + (NADP^+)]$, and of steady state for Calvin cycle intermediates despite large changes in concentrations of some intermediates, notably RuBP and 3-PGA, being implicit in the model's derivation.

Thirdly, the available evidence suggests that the many kinetic constraints on metabolic carbon flow are exquisitely coordinated (Raghavendra & Padmasree 2003; Noctor, De Paepe & Foyer 2006; Rasmusson & Escobar 2007). Any effective model of respiration should at least attempt to capture this coordination. This could be done from the bottom up, by explicitly describing the many regulatory 'throttles' available to plant cells – for example, control of mitochondrial electron transport and reactions of glycolysis by adenylates, negative feedback inhibition of mitochondrial NAD(P)H dehydrogenases by NADH, redox regulation of alternative oxidase, and inactivation of pyruvate decarboxylase in the light by phosphorylation. We refer readers to the several excellent reviews and textbooks on the subject (Buchanan *et al.* 2000; Atkin & Tjoelker 2003; Noctor *et al.* 2006; Plaxton & Podesta 2006; Rasmusson & Escobar 2007; Lambers *et al.* 2008). Our model captures this coordination from the top down, by applying a single synthetic hypothesis, rather than by attempting to describe this vast array of regulatory processes.

Alternatively, if the input parameters describing anabolic and maintenance demands are viewed as empirical constraints, then the many implicit assumptions about metabolic coordination are *necessarily* correct – that is, they are corollaries of the assumed biosynthetic stoichiometries. The challenge then is to exclude demand vectors that are not realistic because they impose flux balance demands on metabolism that cannot be met due to internal kinetic or capacity constraints. From this perspective, our model is a tool for deducing the implications of hypotheses about intracellular energy and carbon flows. It is another matter to extend the model to a predictive regime in which demands estimated from leaf composition can be used to predict and attribute CO_2 fluxes. That would require, at a minimum, better estimates of the diel variation in anabolic rates, and in the spectrum of anabolic products.

Ultimately, we feel that our model should be viewed as a research tool whose purpose is to focus questions that, if answered by experiment, will improve our ability to reliably attribute and predict CO_2 fluxes in intact leaves and at larger scales.

CONCLUSIONS

A stoichiometric flux balance model of leaf respiration, coupled to a biochemical model of photosynthesis, reproduces many generic features of the suppression of non-photorespiratory CO_2 efflux (R_c) by light. These include highly variable suppression by light, enhanced suppression in leaves with low anabolic demands, a two-phase decline in

R_c that is steep at very low PPFD and more gradual at moderate PPFD, reduced O_2 consumption and enhanced CO_2 release during nitrate reduction and a Kok effect (discrete change in apparent quantum yield at low PPFD) that scales with dark respiration rate. The two most important factors governing variation in these features are variation in anabolic demands with PPFD and among plants, and the numerical value of the photosynthetic ATP : $2e^-$ ratio (p_e). The model suggests that effects of PPFD on R_c are driven largely by changes in photosynthetic adenylate balance, which mediates the effects of both photorespiratory NADH retention in mitochondria and export of excess photoreductant. Photorespiration suppression of R_c is predicted only at sub-saturating PPFD. The model suggests that mitochondria are needed to consume excess photoreductant at high PPFD, although photoreductant export is limited by adenylate balance constraints on photosynthetic electron flow. Shifting adenylate balance at high PPFD also suppresses oxidative phosphorylation by flux-balance in the model. This requires engagement of alternative oxidase or uncoupling protein to reduce the P : O ratio, beginning at PPFDs near the transition to RuBP carboxylation limitation. Our model can help focus experimental research on respiration in the light, and provides a framework for assimilating new knowledge, offering the prospect of a tractable, process-based and complete predictive model of leaf CO_2 flux.

ACKNOWLEDGMENTS

T.N.B. thanks Owen Atkin, David Day, Graham Farquhar and Hendrik Poorter for helpful discussions, two anonymous reviewers for very helpful comments on an earlier draft, and Phil Polglase and support staff at Ensis, Yarralumla (now CSIRO Sustainable Ecosystems) for providing office space and support during the early development of this work. This research was supported by the Bushfire Cooperative Research Centre (Australia).

REFERENCES

- Allen J.F. (2003) Cyclic, pseudocyclic and noncyclic photophosphorylation: new links in the chain. *Trends in Plant Science* **8**, 15–19.
- Amirsadeghi S., Robson C.A., McDonald A.E. & Vanlerberghe G.C. (2006) Changes in plant mitochondrial electron transport alter cellular levels of reactive oxygen species and susceptibility to cell death signaling molecules. *Plant & Cell Physiology* **47**, 1509–1519.
- Amthor J.S. (2000) The McCree-de Wit-Penning de Vries-Thornley respiration paradigms: 30 years later. *Annals of Botany* **86**, 1–20.
- Amthor J.S., Goulden M.L., Munger J.W. & Wofsy S.C. (1994) Testing a mechanistic model of forest-canopy mass and energy exchange using eddy correlation: carbon dioxide and ozone uptake by a mixed-oak stand. *Australian Journal of Plant Physiology* **21**, 623–651.
- Anten N.P.R. & Hirose T. (1998) Biomass allocation and light partitioning among dominant and subordinate individuals in *Xanthium canadense* stands. *Annals of Botany* **82**, 665–673.
- Aslam M., Huffaker R.C., Rains D.W. & Rao K.P. (1979) Influence of light and ambient carbon dioxide concentration on nitrate assimilation by intact barley seedlings. *Plant Physiology* **63**, 1205–1209.
- Atkin O.K. & Tjoelker M.G. (2003) Thermal acclimation and the dynamic response of plant respiration to temperature. *Trends in Plant Science* **8**, 343–351.
- Atkin O.K., Westbeek M.H.M., Cambridge M.L., Lambers H. & Pons T.L. (1997) Leaf respiration in light and darkness. A comparison of slow- and fast-growing *Poa* species. *Plant Physiology* **113**, 961–965.
- Atkin O.K., Evans J.R. & Siebke K. (1998) Relationship between the inhibition of leaf respiration by light and enhancement of leaf dark respiration following light treatment. *Australian Journal of Plant Physiology* **25**, 437–443.
- Atkin O.K., Evans J.R., Ball M.C., Lambers H. & Pons T.L. (2000) Leaf respiration of snow gum in the light and dark. Interactions between temperature and irradiance. *Plant Physiology* **122**, 915–923.
- Azcón-Bieto J. & Osmond C.B. (1983) Relationship between photosynthesis and respiration. The effect of carbohydrate status on the rate of CO_2 production by respiration in darkened and illuminated wheat leaves. *Plant Physiology* **71**, 574–581.
- Bartoli C.G., Gomez F., Gergoff G., Guíamét J.J. & Puntarulo S. (2005) Up-regulation of the mitochondrial alternative oxidase pathway enhances photosynthetic electron transport under drought conditions. *Journal of Experimental Botany* **56**, 1269–1276.
- Bernacchi C.J., Singsaas E.L., Pimentel C., Portis A.R.J. & Long S.P. (2001) Improved temperature response functions for models of Rubisco-limited photosynthesis. *Plant, Cell & Environment* **24**, 253–259.
- Bloom A.J., Caldwell R.M., Finazzo J., Warner R.L. & Weissbart J. (1989) Oxygen and carbon dioxide fluxes from barley shoots depend on nitrate assimilation. *Plant Physiology* **91**, 352–356.
- Brooks A. & Farquhar G.D. (1985) Effect of temperature on the CO_2/O_2 specificity of Ribulose-1,5-bisphosphate carboxylase/oxygenase and the rate of respiration in the light. Estimates from gas-exchange measurements on spinach. *Planta* **165**, 397–406.
- Buchanan B.B. (1980) Role of light in the regulation of chloroplast enzymes. *Annual Review of Plant Physiology* **31**, 341–374.
- Buchanan B.B., Gruissem W. & Jones R.L. (2000) *Biochemistry and Molecular Biology of Plants*. American Society of Plant Physiologists, Rockville, MD, USA.
- Caird M.A., Richards J.H. & Donovan L.A. (2007) Nighttime stomatal conductance and transpiration in C_3 and C_4 plants. *Plant Physiology* **143**, 4–10.
- Cannell M.G.R. & Thornley J.H.M. (2000) Modelling the components of plant respiration: some guiding principles. *Annals of Botany* **85**, 45–54.
- Cornic G. & Jarvis P.G. (1972) Effects of oxygen on CO_2 exchange and stomatal resistance in Sitka spruce and maize at low irradiances. *Photosynthetica* **6**, 225–239.
- DeLucia E.H., Drake J.E., Thomas R.B. & Gonzalez-Meler M. (2007) Forest carbon use efficiency: is respiration a constant fraction of gross primary production? *Global Change Biology* **13**, 1157–1167.
- Easlon H.M. & Richards J.H. (2009) Photosynthesis affects following night leaf conductance in *Vicia faba*. *Plant, Cell & Environment* **32**, 58–63.
- Epron D. (1997) The temperature dependence of photoinhibition in leaves of *Phaseolus vulgaris* (L.). Influence of CO_2 and O_2 concentrations. *Plant Science* **124**, 1–8.
- Escobar M.A., Geisler D.A. & Rasmusson A.G. (2006) Reorganization of the alternative pathways of the Arabidopsis respiratory

- chain by nitrogen supply: opposing effects of ammonium and nitrate. *The Plant Journal* **45**, 775–788.
- Farquhar G.D. & Wong S.C. (1984) An empirical model of stomatal conductance. *Australian Journal of Plant Physiology* **11**, 191–210.
- Farquhar G.D., von Caemmerer S. & Berry J.A. (1980) A biochemical model of photosynthetic CO₂ assimilation in leaves of C₃ species. *Planta* **149**, 78–90.
- Farr T.J., Huppe H.C. & Turpin D.H. (1994) Coordination of chloroplastic metabolism in N-limited *Chlamydomonas reinhardtii* by redox modulation. *Plant Physiology* **105**, 1037–1042.
- Finnegan P.M., Soole K.L. & Umbach A.L. (2004) Alternative mitochondrial electron transport proteins in higher plants. In *Plant Mitochondria: From Genome to Function* (eds D.A. Day, A.H. Millar & J. Whelan) pp. 163–230. Kluwer Academic Publishers, Dordrecht, the Netherlands.
- Fritz C., Mueller C., Matt P., Feil R. & Stitt M. (2006) Impact of the C-N status on the amino acid profile in tobacco source leaves. *Plant, Cell & Environment* **29**, 2055–2076.
- Gessler A., Keitel C., Kodama N., Weston C., Winters A.J., Keith H., Grice K., Leuning R. & Farquhar G.D. (2007) ¹³C of organic matter transported from the leaves to the roots in *Eucalyptus delegatensis* – short-term variations and relation to respired CO₂. *Functional Plant Biology* **34**, 692–706.
- Gnaiger E., Méndez G. & Hand S.C. (2000) High phosphorylation efficiency and depression of uncoupled respiration in mitochondria under hypoxia. *Proceedings of the National Academy of Sciences of the United States of America* **97**, 11080–11085.
- Greer D.H., Ottander C. & Öquist G. (1991) Photoinhibition and recovery of photosynthesis in intact barley leaves at 5 and 20 °C. *Physiologia Plantarum* **81**, 203–210.
- Hanning I. & Heldt H.W. (1993) On the function of mitochondrial metabolism during photosynthesis in spinach (*Spinacia oleracea* L.) leaves. *Plant Physiology* **103**, 1147–1154.
- Haraux F. & de Kouchkovsky Y. (1998) Energy coupling and ATP synthase. *Photosynthesis Research* **57**, 231–251.
- Hauschild R. & von Schaewen A. (2003) Differential regulation of glucose-6-phosphate dehydrogenase isoenzyme activities in potato. *Plant Physiology* **133**, 47–62.
- Heber U. (2002) Irrungen, Wirungen? The Mehler reaction in relation to cyclic electron transport in C₃ plants. *Photosynthesis Research* **73**, 223–231.
- Heineke D., Riens B., Grosse H., Hoferichter P., Peter U., Flüge U.-I. & Heldt H.W. (1991) Redox transfer across the inner chloroplast envelope membrane. *Plant Physiology* **95**, 1131–1137.
- Hinkle P.C. (2005) P/O ratios of mitochondrial oxidative phosphorylation. *Biochimica et Biophysica Acta* **1706**, 1–11.
- Hoefnagel M.H.N., Atkin O.K. & Wiskich J.T. (1998) Interdependence between chloroplasts and mitochondria in the light and the dark. *Biochimica et Biophysica Acta* **1366**, 235–255.
- Hurry V., Tobiasson M., Krömer S., Gardeström P. & Öquist G. (1995) Mitochondria contribute to increased photosynthetic capacity of leaves of winter rye (*Secale cereale* L.) following cold-hardening. *Plant, Cell & Environment* **18**, 69–76.
- Hurry V., Keerberg O., Pärnik T., Öquist G. & Gardeström P. (1996) Effect of cold hardening on the components of respiratory decarboxylation in the light and in the dark of leaves of winter rye. *Plant Physiology* **111**, 713–719.
- Ishii R. & Murata Y. (1978) Further evidence of the Kok effect in C₃ plants and the effects of environmental factors on it. *Japanese Journal of Crop Science* **47**, 547–550.
- Jordan D.B. & Ogren W.L. (1984) The CO₂/O₂ specificity of ribulose-1,5-bisphosphate carboxylase/oxygenase: dependence on ribulose bisphosphate concentration, pH and temperature. *Planta* **161**, 308–313.
- Kaiser W.M., Weiner H. & Huber S.C. (1999) Nitrate reductase in higher plants: a case study for transduction of environmental stimuli into control of catalytic activity. *Physiologia Plantarum* **105**, 385–390.
- Kirschbaum M.U.F. (1984) *The Effects of Light, Temperature, and Water Stress on Photosynthesis in Eucalyptus Pauciflora*. Australian National University, Canberra, Australia.
- Kirschbaum M.U.F. & Farquhar G.D. (1987) Investigation of the CO₂ dependence of quantum yield and respiration in *Eucalyptus pauciflora*. *Plant Physiology* **83**, 1032–1036.
- Kok B. (1948) A critical consideration of the quantum yield of *Chlorella* – photosynthesis. *Enzymologia* **13**, 1–56.
- Krause G.H. (1988) Photoinhibition of photosynthesis. An evaluation of damaging and protective mechanisms. *Physiologia Plantarum* **74**, 566–574.
- Krömer S. (1995) Respiration during photosynthesis. *Annual Review of Plant Physiology and Plant Molecular Biology* **46**, 45–70.
- Krömer S. & Heldt H.W. (1991a) On the role of mitochondrial oxidative phosphorylation in photosynthesis metabolism as studied by the effect of oligomycin on photosynthesis in protoplasts and leaves of barley (*Hordeum vulgare*). *Plant Physiology* **95**, 1270–1276.
- Krömer S. & Heldt H.W. (1991b) Respiration of pea leaf mitochondria and redox transfer between the mitochondrial and extramitochondrial compartment. *Biochimica et Biophysica Acta* **1057**, 42–50.
- Krömer S., Stitt M. & Heldt H.W. (1988) Mitochondrial oxidative phosphorylation participating in photosynthetic metabolism of a leaf cell. *FEBS Letters* **226**, 352–356.
- Kruse J. & Adams M.A. (2008) Three parameters comprehensively describe the temperature response of respiratory oxygen reduction. *Plant, Cell & Environment* **31**, 954–967.
- Lambers H., Chapin F.S. & Pons T.L. (2008) *Plant Physiological Ecology*. 2nd edn, Springer, New York, USA.
- Lee C.P., Gu Q., Xiong Y., Mitchell R.A. & Ernster L. (1996) P/O ratios reassessed: mitochondrial P/O ratios consistently exceed 1.5 with succinate and 2.5 with NAD-linked substrates. *Journal of the Federation of American Societies for Experimental Biology* **10**, 345–350.
- McDonald E.P., Erickson J.E. & Kruger E.L. (2002) Can decreased transpiration limit plant nutrient acquisition in elevated CO₂? *Functional Plant Biology* **29**, 1115–1120.
- Matos A.R., Hourton-Cabassa C., Çiçek D., Reze N., Arrabaça J.D., Zachowski A. & Moreau F. (2007) Alternative oxidase involvement in cold stress response of *Arabidopsis thaliana fad2* and *FAD3+* cell suspensions altered in membrane lipid composition. *Plant & Cell Physiology* **48**, 856–865.
- Mizuno N., Sugie A., Kobayashi F. & Takumi S. (2007) Mitochondrial alternative pathway is associated with development of freezing tolerance in common wheat. *Journal of Plant Physiology* **165**, 462–467.
- Noctor G. & Foyer C.H. (1998) A re-evaluation of the ATP:NADPH budget during C₃ photosynthesis: a contribution from nitrate assimilation and its associated respiratory activity? *Journal of Experimental Botany* **49**, 1895–1908.
- Noctor G., De Paepe R. & Foyer C.H. (2006) Mitochondrial redox biology and homeostasis in plants. *Trends in Plant Science* **12**, 125–134.
- Noguchi K., Taylor N.L., Millar A.H., Lambers H. & Day D.A. (2005) Response of mitochondria to light intensity in the leaves of sun and shade species. *Plant, Cell & Environment* **28**, 760–771.
- Penning de Vries F.W.T., Brunsting A.H.M. & Van Laar H.H. (1974) Products, requirements and efficiency of biosynthesis: a quantitative approach. *Journal of Theoretical Biology* **45**, 339–377.
- Plaxton W.C. & Podesta F.E. (2006) The functional organization and control of plant respiration. *Critical Reviews in Plant Sciences* **25**, 159–198.

- de Pury D.G.G. & Farquhar G.D. (1997) Simple scaling of photosynthesis from leaves to canopies without the errors of big-leaf models. *Plant, Cell & Environment* **20**, 537–557.
- Raghavendra A.S. & Padmasree K. (2003) Beneficial interactions of mitochondrial metabolism with photosynthetic carbon assimilation. *Trends in Plant Science* **8**, 546–553.
- Raghavendra A.S., Padmasree K. & Saradadevi K. (1994) Interdependence of photosynthesis and respiration in plant cells: interactions between chloroplasts and mitochondria. *Plant Science* **97**, 1–14.
- Raghavendra A.S., Reumann S. & Heldt H.W. (1998) Participation of mitochondrial metabolism in photorespiration. Reconstituted system of peroxisomes and mitochondria from spinach leaves. *Plant Physiology* **116**, 1333–1337.
- Rasmusson A.G. & Escobar M.A. (2007) Light and diurnal regulation of plant respiratory gene expression. *Physiologia Plantarum* **129**, 57–67.
- Reed A.J., Canvin D.T., Sherrard J.H. & Hageman R.H. (1983) Assimilation of [¹⁵N]nitrate and [¹⁵N]nitrite in leaves of five plant species under light and dark conditions. *Plant Physiology* **71**, 291–294.
- Reumann S., Heupel R. & Heldt H.W. (1994) Compartmentation studies on spinach leaf peroxisomes. II. Evidence for the transfer of reductant from the cytosol to the peroxisomal compartment via a malate shuttle. *Planta* **193**, 167–173.
- Ribas-Carbo M., Taylor N.L., Giles L., Busquets S., Finnegan P.M., Day D.A., Lambers H., Medrano H., Berry J.A. & Flexas J. (2005) Effects of water stress on respiration in soybean leaves. *Plant Physiology* **139**, 466–473.
- Running S.W. & Coughlan J.C. (1988) A general model of forest ecosystem processes for regional applications 1. Hydrologic balance, canopy gas exchange and primary production processes. *Ecological Modelling* **42**, 125–154.
- Saradadevi K. & Raghavendra A.S. (1992) Dark respiration protects photosynthesis against photoinhibition in mesophyll protoplasts of pea (*Pisum sativum*). *Plant Physiology* **99**, 1232–1237.
- Scheible W.-R., Krapp A. & Stitt M. (2000) Reciprocal diurnal changes of PEPc expression, cytosolic pyruvate kinase, citrate synthase and NADP-isocitrate dehydrogenase expression regulate organic acid metabolism during nitrate assimilation in tobacco leaves. *Plant, Cell & Environment* **23**, 1155–1167.
- Seelert H., Poetsch A., Dencher N.A., Engel A., Stahlberg H. & Müller D.J. (2000) Proton-powered turbine of a plant motor. *Nature* **405**, 418–419.
- Sharp R.E., Matthews M.A. & Boyer J.S. (1984) Kok effect and the quantum yield of photosynthesis. *Plant Physiology* **75**, 95–101.
- Sherameti I., Sopory S.K., Trebicka A., Pfanschmidt T. & Oelmüller R. (2002) Photosynthetic electron transport determines nitrate reductase gene expression and activity in higher plants. *The Journal of Biological Chemistry* **277**, 46594–46600.
- Stitt M., Müller C., Matt P., Gibon Y., Carillo P., Morcuende R., Scheible W.-R. & Krapp A. (2002) Steps towards an integrated view of nitrogen metabolism. *Journal of Experimental Botany* **53**, 959–970.
- Tcherkez G. & Hodges M. (2008) How stable isotopes may help to elucidate primary nitrogen metabolism and its interaction with (photo)respiration in C₃ leaves. *Journal of Experimental Botany* **59**, 1685–1693.
- Tcherkez G., Bligny R., Gout E., Mahe A., Hodges M. & Cornic G. (2008) Respiratory metabolism of illuminated leaves depends on CO₂ and O₂ conditions. *Proceedings of the National Academy of Sciences of the United States of America* **105**, 797–802.
- Thornley J.H.M. (1970) Respiration, growth and maintenance in plants. *Nature* **227**, 304–305.
- Urbanczyk-Wochniak E., Baxter C., Kolbe A., Kopka J., Sweetlove L.J. & Fernie A. (2005) Profiling of diurnal patterns of metabolite and transcript abundance in potato (*Solanum tuberosum*) leaves. *Planta* **221**, 891–903.
- Villar R., Held A.A. & Merino J. (1995) Dark leaf respiration in light and darkness of an evergreen and a deciduous plant species. *Plant Physiology* **107**, 421–427.
- Waring R.H., Landsberg J.J. & Williams M. (1998) Net primary production of forests: a constant fraction of gross primary production? *Tree Physiology* **18**, 129–134.
- Williams M., Rastetter E.B., Fernandes D.N., Goulden M.L., Wofsy S.C., Shaver G.R., Melillo J.M., Munger J.W., Fan S.M. & Nadelhoffer K.J. (1996) Modelling the soil-plant-atmosphere continuum in a Quercus-Acer stand at Harvard Forest: the regulation of stomatal conductance by light, nitrogen and soil/plant hydraulic properties. *Plant, Cell & Environment* **19**, 911–927.
- Willms J.R., Dowling A.N., Dong Z.-M., Hunt S., Shelp B. & Layzell D.B. (1997) The simultaneous measurement of CO₂ and O₂ exchange in biological systems. *Analytical Biochemistry* **254**, 272–282.
- Wullschlegel S.D. (1993) Biochemical limitations to carbon assimilation in C₃ plants – A retrospective analysis of the A/c₃ curves from 109 species. *Journal of Experimental Botany* **44**, 907–920.
- Yoshida K., Terashima I. & Noguchi K. (2007) Up-regulation of mitochondrial alternative oxidase concomitant with chloroplast over-reduction by excess light. *Plant & Cell Physiology* **48**, 606–614.

Received 10 May 2010; received in revised form 25 August 2010; accepted for publication 26 August 2010

SUPPORTING INFORMATION

Additional Supporting Information may be found in the online version of this article:

Supporting information Calculation of anabolic demand terms.

Table S1. Gross stoichiometries for biosynthesis of eight amino acids and their carbon skeleton precursors. Numbers shown are the number of molecules of the compound in the column heading that are consumed in the synthesis of one molecule of the compound named in the first column. Positive numbers represent net yield rather than consumption. Net stoichiometries are given in Table S2.

Table S2. Net stoichiometries for biosynthesis of eight amino acids, and the percent of total amino acids contributed by each in calculations of anabolic demand/supply terms.

Table S3. Net production of NADH, NADPH, ATP and CO₂ per mole of source carbon in the biosynthesis and maintenance of five classes of compounds used to calculate anabolic demand in the current study. Dimensions are moles of NADH, NADPH, CO₂ or ATP per mole of source carbon consumed in biosynthesis of products listed in the column headings. Two values are given for NADH and NADPH, based on nitrogen assimilation beginning from either nitrate or ammonium (N assimilation affects stoichiometries for phospholipid synthesis here because we used phosphatidyl serine as the archetype for phosphate-linked R group). Three values are given for ATP under the heading of protein. For biosynthesis, (1) represents de novo synthesis of amino acids only; and (2) represents both

de novo synthesis and polymerisation of amino acids. For maintenance, (3) represents degradation of proteins and repolymerisation of existing amino acids only. Calculations are described above under 'Supply/demand stoichiometries for biosynthesis and maintenance processes.'

Please note: Wiley-Blackwell are not responsible for the content or functionality of any supporting materials supplied by the authors. Any queries (other than missing material) should be directed to the corresponding author for the article.

APPENDIX

Model derivation

The model is derived from stoichiometric constraints on the ATP, NADH, chloroplastic and cytosolic NADPH, CO₂ and O₂ fluxes that arise from biosynthesis, maintenance and photosynthesis, under the assumption that metabolic intermediates – not products – are in steady-state. In other words, we assume that metabolic carbon flow and the associated adenylate and reductant cycling and gas exchange are determined entirely by demand for anabolic products and energy carriers. Those demands are treated as input parameters or are calculated from the photosynthesis model of Farquhar *et al.* (1980). This assumption allows us to create and solve a set of steady-state supply/demand equations for adenylates and reductants. We then calculate fluxes of CO₂ and O₂ from the solution. A heuristic diagram of the model, meant to aid the reader in following the derivation below, is given in Fig. 1.

We assume that all reduced carbon comes either from sucrose, starch, or triose phosphates (TP), but that photosynthetically derived TP is the preferred C source for anabolic demands because of the ATP cost of accessing stored carbohydrates. Carbon flow from these sources is separated into five streams. The first stream, termed *catabolic carbon flow*, is the rate of carbon flow to CO₂ via glycolysis and the tricarboxylic acid (TCA) cycle that is not attributable to anabolic carbon processing; we use the symbol V_{cat} to denote this stream. The second stream is flow through the chloroplastic oxidative pentose phosphate pathway (OPPP) to CO₂ at a rate V_{opp} . The third is flow through the cytosolic OPPP to CO₂ at a rate V_{opc} . The fourth is flow into anabolic products at a rate V_{ana} and the fifth is flow to CO₂ as a by-product of flows into anabolic products, at a rate V_{by} . This fifth stream represents CO₂ lost in pyruvate decarboxylation or in intermediate steps of the TCA cycle when carbon atoms remaining in decarboxylated compounds end up in anabolic products rather than being fully oxidised to CO₂.

We define five terms representing energy carrier supply or demand not arising from photosynthesis or photorespiration. Four of these terms arise from anabolic carbon flow (biosynthesis): B_t , B_n , B_p and B_c , which denote, respectively, ATP demand, chloroplastic NADPH demand, cytosolic NADPH demand and NADH supply. Because, and on balance, more NADH is usually produced than consumed during anabolism, B_n is expressed as a supply, so that it is

typically positive. This may appear confusing, but it makes the solution easier to interpret. B_t includes ATP costs of *de novo* biosynthesis, turnover biosynthesis and, where relevant, polymerisation. A fifth term, M , representing 'maintenance' ATP demands, includes repolymerisation of existing amino acids and maintenance of ion gradients. In the *Supporting Information*, we provide a brief justification of numerical values assigned to these terms in our simulations, based on major biosynthetic and maintenance demands estimated from leaf composition data.

These anabolic and maintenance supply/demand terms are combined with similar terms that account for ATP synthesis and NADH oxidation in mitochondria, ATP and photoreductant supply and demand associated with photosynthesis and photorespiration, and export of redox equivalents from chloroplasts. All of these terms are brought together to create steady-state supply/demand equations (flux-balance equations) for energy carriers. The simultaneous solution of these equations yields expressions for net non-photorespiratory CO₂ release and O₂ consumption. Expressions also arise for the maximum and actual P : O ratios for oxidative phosphorylation, from which we can infer the relative involvement of non-phosphorylating pathways in mitochondrial electron transport). We derive the flux-balance equations below.

NADH/FADH₂. NADH equivalents arise from several sources. First, every 3-C triose-phosphate (TP) molecule entering this stream generates one NADH in glycolysis, one in PDH, and four equivalents in TCA (3 NADH + 1 FADH₂) (FAD accepts electrons from succinate in the sixth step in the TCA cycle; this is discussed under P : O Ratio below). The rate of catabolic production of NADH equivalents is thus $2V_{\text{cat}}$ (2 NADH equivalents per source C atom). Export of excess photoreductant from chloroplasts via the Mal/OAA shuttle also supplies NADH, at a rate V_{px} (discussed under *Chloroplastic NADPH* below). Biosynthetic demand for carbon skeletons drives carbon flow through some steps of glycolysis and the TCA cycle, generating NADH at the rate B_n . NADH is consumed by oxidation at the mitochondrial electron transport chain (mETC). Finally, the rate of NADH consumption equals $2R_o$, where R_o is the rate of O₂ reduction by the mETC.

In photorespiratory conditions, NADH is also generated via Gly decarboxylation in mitochondria at a rate $0.5\phi V_c$, where V_c is the rate of RuBP carboxylation and ϕ is the ratio of oxygenation to carboxylation rate. The fate of this NADH is important but uncertain. An equal amount of NADH is needed to reduce hydroxypyruvate to glycerate in peroxisomes, and since NADH can be shuttled between organelles and the cytosol via the Mal/OAA shuttle (Heineke *et al.* 1991; Reumann, Heupel & Heldt 1994; Hoefnagel *et al.* 1998), it seems inconsistent to exclude such shuttling from a model based on stoichiometric flux balance. However, the few available data (Krömer & Heldt 1991b; Hanning & Heldt 1993) indicate that only 25–50% of photorespiratory NADH is exported to peroxisomes; the remainder remains in mitochondria and can contribute

electrons to the mETC. We address this issue by assuming a fraction f_m (nominally 0.5) of photorespiratory NADH remains in mitochondria. The limiting case of unlimited NADH transfer between mitochondria and peroxisomes can be assessed by setting $f_m = 0$. The steady state supply/demand equation for NADH equivalents is then found by setting source terms (at left) equal to sink terms (at right):

$$2V_{\text{cat}} + B_n + V_{\text{px}} + \frac{1}{2}f_m\phi V_c = 2R_o. \quad (\text{A1})$$

Chloroplastic NADPH. There are two sources and four sinks for chloroplastic reductant. Linear photosynthetic electron transport at a rate J_a generates NADPH at a rate $J_a/2$. The chloroplastic oxidative pentose phosphate pathway (OPPP) generates 6 NADPH and 3 CO₂ per TP, so the NADPH production rate is $2V_{\text{opp}}$. NADPH is consumed by the Calvin cycle at the rate $(2 + 2\phi)V_c$ (FCB). Anabolism also consumes NADPH in chloroplasts, at the rate B_p . Chloroplasts must also export reducing equivalents to peroxisomes at a rate $0.5f_m\phi V_c$ to make up for the fraction of photorespiratory NADH that remains in mitochondria. Finally, at high light, excess photoreductant can be exported via the Mal/OAA shuttle, at a rate V_{px} . The steady state supply/demand equation for chloroplastic NADPH is then

$$2V_{\text{opp}} + \frac{1}{2}J_a = \omega V_c + B_p + V_{\text{px}}, \quad (\text{A2})$$

where $\omega = 2 + 2\phi + 0.5f_m\phi$. Note that Eqn A2 is a generalisation of the FCB model. Under RuBP limited conditions, FCB predicts V_c by setting photoreductant demand $(2 + 2\phi)V_c$ equal to supply $(J_a/2)$. Equation 2 extends that model to account for anabolic reductant demands (B_p), catabolic reductant supply (V_{opp}) and reductant export (V_{px}). The latter two variables are undetermined, so we require two additional constraints to solve Eqn A2. Chloroplastic glucose-6-phosphate dehydrogenase (G6PDH), the key regulatory enzyme in the OPPP, is strongly redox inhibited in the light (Buchanan 1980). The precise light dependence of this inhibition in higher plants is unknown, but in single-celled algae studied by Farr *et al.* (1994), inhibition was evident at $5 \mu\text{E m}^{-2} \text{s}^{-1}$ and complete by $10\text{--}20 \mu\text{E m}^{-2} \text{s}^{-1}$. We assume that the chloroplastic OPPP is downregulated in proportion to increasing thylakoid electron transport rate, so that reductant supply never falls below anabolic demand. This implies:

$$V_{\text{opp}} = \frac{1}{4} \max\{0, 2B_p - J\}, \quad (\text{A3})$$

where J_a has been replaced by J , potential electron transport rate, because $J_a = J$ at low light. Equation A3 implies that CO₂ release in the chloroplastic OPPP is fully inhibited when $J \geq 2B_p$; however, it does not preclude activity of reversible components of the OPPP in the light for the production of carbon skeletons (Hauschild & von Schaewen 2003). It also implies that NADPH generation in this

narrow range of low light ($0 < J < 2B_p$) serves only to supplant OPPP activity, so that no net carboxylation of RuBP occurs in this range. Whether this actually occurs is unknown; it is a prediction of the model.

Photoreductant supply can exceed anabolic and Calvin cycle demand at high light, in which case chloroplasts may export excess reductant to maintain flux balance. The *potential* excess rate of NADPH generation is found by applying $V_{\text{opp}} = V_{\text{px}} = 0$ and $J_a = J$ to Eqn A2 to give $J/2 + 2V_{\text{opp}} - B_p - \omega V_c$. It is unclear how much of this excess actually generates NADPH, because energy can be dissipated by other mechanisms (e.g. the xanthophyll cycle and fluorescence). We assume a fraction (f_x) of excess reducing potential generates excess NADPH that is exported; another constraint on f_x emerges below, in *Flux balance constraints on P : O ratio and photoreductant export*. The export term V_{px} in Eqn A1 is then given by:

$$V_{\text{px}} = f_x \cdot \max\left\{0, \frac{1}{2}J + 2V_{\text{opp}} - B_p - \omega V_c\right\}. \quad (\text{A4})$$

Finally, J_a must satisfy Eqn A2, so

$$J_a = 2(B_p + \omega V_c + V_{\text{px}} - 2V_{\text{opp}}) \quad (\text{A5})$$

Cytosolic NADPH

We consider only one source and one sink for cytosolic NADPH. The cytosolic OPPP generates NADPH at a rate $2V_{\text{opc}}$, and anabolic demand consumes cytosolic NADPH at the rate B_c . We assume these two processes are perfectly coupled; i.e. the cytosolic OPPP operates only to satisfy anabolic demands for NADPH in the cytosol, and that it does not contribute significant reductant flows to the mETC. Thus,

$$V_{\text{opc}} = \frac{1}{2}B_c \quad (\text{A6})$$

All of the anabolic NADPH demands accounted for in this paper are localised within chloroplasts, so V_{opc} plays no role in the simulations shown here. It is included only for completeness.

ATP

We consider three sources of ATP. Catabolic carbon flow through glycolysis and the TCA cycle generates three ATP per triose phosphate (one per C), so the rate of ATP generation equals the rate of carbon flow, or V_{cat} . Oxidative phosphorylation yields ATP at a rate given by the product of the O reduction rate ($2R_o$) and the P : O ratio (p_o , the ratio of ADP phosphorylation rate to O reduction rate). p_o is discussed in detail below. Photophosphorylation generates ATP at a rate $0.5p_e J_a$, where p_e is the number of ADP phosphorylated per two electrons flowing through the photosynthetic electron transport chain (often denoted 'ATP : 2e⁻'). p_e may vary and can be enhanced by cyclic electron transport around PSI; in the absence of cyclic flow

it is probably between 3/2 (1.5) and 9/7 (~1.286). These values assume either 12 or 14 protons, respectively, per 3 ATP, and 12 protons per four electrons (Seelert *et al.* 2000; Allen 2003). We will use the larger value for p_e by default, but will compare the resulting predictions with simulations based on $p_e = 1.286$.

ATP is consumed by biosynthesis and maintenance at the rates B_t and M , respectively. The Calvin cycle and photorespiration together consume ATP at a rate $(3 + 3.5\phi)V_c$ (FCB). ATP is also needed to store or export excess photosynthate or to access stored carbohydrate. Starch synthesis consumes one ATP per 6-C sugar, as does sucrose synthesis and export in apoplasmic phloem loaders. Starch breakdown consumes two ATP per 6-C sugar. Sucrose breakdown consumes one or two ATP equivalents, via the sucrose synthase and invertase routes, respectively; we assume the latter. Denoting the combined *net* rate of sucrose export and starch synthesis as S (note $S = V_c - 0.5V_o - V_{ana}$, the difference between photosynthetic yield and anabolic carbon flow), the net ATP demand is tS , where $t = -1/3$ if $S < 0$ and $+1/6$ if $S > 0$ (note $tS > 0$ in either case). The steady state supply/demand equation for ATP is then:

$$2p_o R_o + V_{cat} + \frac{1}{2} p_e J_a = B_t + M + (3 + 3.5\phi)V_c + tS \quad (A7)$$

P : O ratio (p_o)

The stoichiometry of ATP production and e^- flow to O_2 in mitochondria depends on two factors: where electrons are donated to the mETC, and the activities of non-phosphorylating pathways. Electrons donated at Complex I yield a maximum of 2.3–3 ATP per O reduced, whereas electrons donated elsewhere net up to 1.4–2 ATP per O reduced. The range of quoted values reflects disagreement in the literature (Lee *et al.* 1996; Gnaiger, Méndez & Hand 2000; Hinkle 2005). Lesser ratios are considered ‘mechanistic’ inasmuch as they are derived from experiments on isolated mitochondria, whereas greater ratios are predicted by theory. We use intermediate values (1.5 and 2.5, or 3/2 and 5/2, respectively), and assume that cytosol-derived NADH is shuttled to the matrix via the Mal/OAA shuttle and donates its electrons at Complex I. The maximum P : O ratio then depends only on the proportional contribution of FADH₂. (FADH₂ is not labile, and it donates its electrons at Complex II in the mitochondrial inner membrane. Transport of those electrons to cytochrome oxidase can transport a maximum of $6H^+ - 4$ fewer than possible for electrons from NADH oxidation at Complex I. FADH₂ therefore supports a lower rate of ATP production.) The maximum P : O ratio, p_{om} , is a reductant flow weighted average of these two values, where the individual flows are the positive terms in Eqn A1 ($2V_{cat}$, B_n , V_{px} and $0.5f_m\phi V_c$). In purely catabolic oxidation of carbohydrates, one of six reducing equivalents is FADH₂, so the maximum P : O for V_{cat} is $(1/6) \cdot (3/2) + (5/6) \cdot (5/2)$, or 7/3. Since oxaloacetic acid (OAA) is the only TCA intermediate downstream of

FADH₂ that is consumed in anabolic processes that we account for in this paper, and since we assume OAA is generated by PEP carboxylation for that purpose, we can consider all redox equivalents generated as a by-product of anabolic carbon flow as NADH. Therefore the larger P : O-value (5/2) applies to B_n . The same is true for redox equivalents exported from chloroplasts and for NADH generated in mitochondria by photorespiratory Gly conversion, so the 5/2-value applies to V_{px} and $0.5f_m\phi V_c$ as well. The effective maximum P : O ratio is then:

$$p_{om} = \frac{\frac{7}{3}(2V_{cat}) + \frac{5}{2}(B_n + V_{px} + \frac{1}{2}f_m\phi V_c)}{2V_{cat} + B_n + V_{px} + \frac{1}{2}f_m\phi V_c} \quad (A8)$$

Flux balance constraints on P : O ratio and photoreductant export

If reductant supply to the mETC exceeds ADP supply, flux balance can be maintained in one of two ways: by reducing NADH and ATP supply from catabolic substrate oxidation or by reducing the P : O ratio, perhaps by increased engagement of AOX or uncoupling protein. There is evidence that AOX activity is strongly enhanced by stress (Finnegan, Soole & Umbach 2004), including water stress (Bartoli *et al.* 2005; Ribas-Carbo *et al.* 2005), low temperatures (Matos *et al.* 2007; Mizuno *et al.* 2007) and excess light (Noguchi *et al.* 2005; Yoshida, Terashima & Noguchi 2007), and that it serves as a supplementary electron sink, probably to regenerate NAD⁺ and/or to prevent generation of reactive oxygen species (Amirsadeghi *et al.* 2006). A core hypothesis of our model is that p_o is downregulated to maintain flux balance, first by reducing TCA cycle activity, and then by downregulation of p_o . We implement this hypothesis with a conditional statement: if flux balance requires $V_{cat} < 0$ in Eqn A7, then V_{cat} is zero and flux balance is maintained by reducing p_o below p_{om} . This conditional statement is formally expressed by Eqn A13 below.

However, although reducing p_o to zero can permit a continued increase in oxidation of redox equivalents by the mETC, it cannot ensure adenylate balance if ATP supply continues to increase – as, for example, may occur in chloroplasts at high light. This requires an additional constraint on adenylate balance, beyond those already explicit in Eqn A7. The only arbitrary term in Eqn A7 is the parameter f_x , the fraction of excess thylakoid reducing potential that is dissipated via NADPH export. Photoreductant export affects adenylate balance because photosynthetic e^- transport is inextricably coupled to photophosphorylation. Thus, when $p_o = 0$, adenylate balance places a constraint on thylakoid electron transport rate, J_a :

$$J_a \leq 2(B_t + M + tS + (3 + 3.5\phi)V_c)/p_e, \quad (A9)$$

which is found by setting $p_o = V_{cat} = 0$ in Eqn A7. Substituting A4 into A5, setting $V_{opp} = 0$, applying the result to A9 and solving for f_x gives

$$f_x = \min \left\{ 1, \frac{B_t + M + tS - p_c B_p + (3 + 3.5\phi - p_c \omega) V_c}{p_c \left(\frac{1}{2} J - B_p - \omega V_c \right)} \right\}. \quad (\text{A10})$$

This produces negative or undefined values at low light (e.g. when $J \leq 2B_p$), but in this case V_{px} is zero, so the value of f_x is irrelevant in such cases.

Solution

Non-photorespiratory CO_2 release (R_c) arises in four ways: by chloroplastic and cytosolic OPPP activity at rates V_{opp} and V_{opc} , respectively; by catabolic substrate oxidation at a rate V_{cat} , and as a by-product of anabolic carbon flow, at a rate V_{by} . R_c is therefore given by

$$R_c = V_{opp} + V_{opc} + V_{cat} + V_{by}. \quad (\text{A11})$$

(We use the notation R_c to distinguish it from R_n and R_d [the conventional notations for mitochondrial respiration rate at night and in the daytime, respectively], because Eqn A11 is meant to apply either in light or in darkness.) The four terms on the right-hand side of Eqn A11 must be supplied to calculate R_c . V_{by} is a model input, V_{opc} is given by Eqn A6, and V_{opp} is given by Eqns A2–A4, leaving only V_{cat} . To constrain V_{cat} , we will solve Eqns A1 & A7 for V_{cat} by eliminating R_o . We will then use the conditional assumption outlined above under *Flux balance constraints* to eliminate the P : O ratio. Eliminating R_o from Eqns A1 & A7 gives V_{cat} as

$$V_{cat} = B_t + M + tS + (3 + 3.5\phi) V_c - \frac{1}{2} p_c J_a - \left(p_o \left(B_n + V_{px} + \frac{1}{2} f_m \phi V_c \right) \right) / (2p_o + 1). \quad (\text{A12})$$

The requirement that $V_{cat} \geq 0$ and the assumption that $p_o = p_{om}$ if $V_{cat} > 0$ leads to

$$V_{cat} = \max\{V_{cat}^*, 0\}, \quad (\text{A13})$$

where

$$V_{cat}^* = B_t + M + tS + (3 + 3.5\phi) V_c - \frac{1}{2} p_c J_a - \left(p_{om} \left(B_n + V_{px} + \frac{1}{2} f_m \phi V_c \right) \right) / (2p_{om} + 1). \quad (\text{A14})$$

p_{om} is eliminated from Eqn A14 by combining Eqns A8 & A14 and solving for V_{cat} to give

$$V_{cat}^* = \frac{3}{17} \left(B_t + M + tS + (3 + 3.5\phi) V_c - \frac{1}{2} p_c J_a - \frac{5}{2} \left(B_n + V_{px} + \frac{1}{2} f_m \phi V_c \right) \right). \quad (\text{A15})$$

The factor 3/17 arises from $2(7/3) + 1$, which is the denominator after p_{om} has been eliminated (7/3 is the maximum P : O ratio for reductant arising from catabolic substrate oxidation; see *P : O ratio* above). The remaining terms in Eqn A15, and thus in Eqn A11 for R_c , are all given by equations above: V_{px} is given by Eqns A4 & A10, J_a by Eqn A5 and V_c by Eqns A18 & A19 below.

Expressions for the rate of O_2 consumption by mitochondria (R_o), the actual P : O ratio (p_o) and the net rates of CO_2 assimilation (A) and oxygen evolution (A_o) can also be obtained from the equations above, when combined with the FCB model. R_o is found by solving Eqn A1:

$$R_o = V_{cat} + \frac{1}{2} \left(B_n + V_{px} + \frac{1}{2} f_m \phi V_c \right) \quad (\text{A16})$$

p_o is found by solving Eqn A7 for p_o and substituting Eqn A16 for R_o :

$$p_o = \frac{B_t + M + tS + (3 + 3.5\phi) V_c - \frac{1}{2} p_c J_a - V_{cat}}{2V_{cat} + B_n + V_{px} + \frac{1}{2} f_m \phi V_c}. \quad (\text{A17})$$

Note that this equals p_{om} if $V_{cat} > 0$; otherwise, it equals the value of the overall P : O ratio needed to ensure flux balance for both ATP and NADH. From FCB, net CO_2 assimilation rate is $V_c - 0.5V_o - R_c = (1 - 0.5\phi)V_c - R_c$. The rate of RuBP carboxylation (V_c) is the lesser of the RuBP-saturated and -limited rates (W_c and J' , respectively). W_c is given by Eqn 9 in FCB:

$$W_c = \frac{V_m c_i}{c_i + K_c (1 + O/K_o)}, \quad (\text{A18})$$

where K_c and K_o are the Michaelis constants for RuBP carboxylation and oxygenation, respectively, and c_i and O are intercellular CO_2 and ambient O_2 partial pressures, respectively. To find J' , we begin by considering V_c above the light level causing full inhibition of chloroplastic OPPP ($V_{opp} = 0$) but below the level producing excess photoreductant ($V_{px} = 0$). Applying $V_{opp} = V_{px} = 0$ to Eqn A2 gives $V_c = (J/2 - B_p)/\omega$. Generalising this to include the low-light regime in which $V_{opp} > 0$ but $V_c = 0$, we have

$$J' = \max \left\{ 0, \left(\frac{1}{2} J - B_p \right) / \omega \right\}. \quad (\text{A19})$$

We calculate the minimum of W_c and J' hyperbolically to reflect co-limitation near the transition (Farquhar *et al.* 1980): $\theta_v V_c^2 - (W_c + J') V_c + W_c J' = 0$, where θ_v is a dimensionless parameter ($\theta_v = 1$ creates a sharp transition; we used $\theta_v = 0.999$). From FCB, ϕ , the ratio of RuBP oxygenation rate to carboxylation rate, is $0.21(O/K_o)/(c_i/K_c)$. Noting from FCB that $\phi = 2\Gamma^*/c_i$, where Γ^* is the photorespiratory CO_2 compensation point, we have:

$$A = \min \left\{ \frac{\max \left\{ 0, \frac{1}{4}(J - 2B_p) \right\} (c_i - \Gamma_*)}{c_i + \left(2 + \frac{1}{2} f_m \right) \Gamma_*}, \frac{V_m (c_i - \Gamma_*)}{c_i + K_c (1 + O/K_o)} \right\} - R_c. \quad (\text{A20})$$

This differs from the FCB model by two terms, both affecting the RuBP-limited phase: the offset of J by $2B_p$, and the factor $0.5f_m$ multiplied by Γ_* in the denominator. If f_m is on the order of 0.5, as has been reported previously (Krömer & Heldt 1991b), then its effect on the shape of the A vs. c_i curve is negligible. The effect of the B_p term depends on NADPH demand, including the ferredoxin needed to reduce NO_2^- to NH_4^+ in N assimilation. Net photosynthetic O_2 evolution arises from water splitting at PSII and photorespiration. For each RuBP oxygenated, 1.5 O_2 are consumed, so the consumption rate is $1.5V_o$ ($1.5\phi V_c$). The rate

of O_2 evolution from water splitting equals 1/4 of the actual electron transport rate, J_a . Thus, noting that O_2 consumption by the mETC is R_o , the net O_2 evolution rate (A_o) is:

$$A_o = \frac{1}{4} J_a - \frac{3}{2} \phi V_c - R_o \quad (\text{A21})$$

Values are needed for c_i , O , K_c , K_o , V_m and J . We used values for K_c and K_o at 25 °C from Bernacchi *et al.* (2001). We calculated J from incident PPFD (I) and maximum potential e^- transport rate (J_m) as the lesser root of $\theta_j J^2 - (J_m + fI)J + fJ_m I$ (Farquhar & Wong 1984), where $\theta_j = 0.86$ and f ($0.3 e^-/h\nu$) is the product of absorbance and maximum quantum yield. J_m was taken as $2.1 V_m$ (Wullschleger 1993). We estimated V_m from leaf N content, based on the data used to estimate anabolic demands (see *Supporting Information*). c_i , O and I were varied among simulations. These parameter values are given in Table 3.